Table 3 Changes in Biological Function Associated with Changes in Gene Expression in GFP^+ Fibroblasts at 14 Days after Bleomycin Treatment

Function annotation	*P* value	Predicted activation state	Activation *Z*-score
Proliferation of cells	1.19×10^{-42}	Increased	3.075
Necrosis	7.76×10^{-36}		−1.309
Cell death	2.45×10^{-35}		−1.146
Apoptosis	2.86×10^{-34}		−1.598
Cell movement	1.74×10^{-28}	Increased	3.756
Migration of cells	2.78×10^{-28}	Increased	3.179
Metabolism of protein	4.61×10^{-28}	Increased	2.429
Proliferation of fibroblasts	6.11×10^{-22}	Increased	2.54
Invasion of cells	1.96×10^{-20}	Increased	2.798
Proliferation of fibroblast cell lines	4.35×10^{-19}	Increased	2.526
Proliferation of connective tissue cells	2.36×10^{-18}	Increased	3.652
Migration of connective tissue cells	1.32×10^{-16}	Increased	2.843
Cell movement of connective tissue cells	2.77×10^{-16}	Increased	3.032
Migration of fibroblasts	7.95×10^{-16}	Increased	2.253
Cell movement of fibroblasts	5.39×10^{-15}	Increased	2.57
Cell spreading	1.08×10^{-13}	Increased	2.297
Adhesion of connective tissue cells	2.20×10^{-10}	Increased	2.849
Attachment of cells	1.65×10^{-08}	Increased	2.557
Chemotaxis	1.64×10^{-06}	Increased	2.317

Interestingly, most OPN^+ GFP^+ fibroblasts had an activated phenotype with high FSC and SSC (Figure 6B).

We also confirmed the expression of OPN in bleomycin-treated GFP^+ fibroblasts by immunofluorescence staining *in vitro* (Figure 6D) and *in vivo* (Figure 6E). OPN was detected in the cytoplasm around the nucleus, probably associated with the endoplasmic reticulum and intracellular vesicles (Figure 6D). *In vivo*, OPN^+ rounded leukocytes were detected in the alveolar air spaces, possibly representing alveolar macrophages.[42] OPN^+ GFP^+ fibroblasts existed at the boundaries between the alveolar air spaces and the fibrotic region where GFP^+ fibroblasts clustered (Figure 6E). In addition, some OPN^+ GFP^+ fibroblasts were detected adjacent to epithelium-denuded alveoli (Figure 6E). Some but not all OPN^+ GFP^+ fibroblasts coexpressed α-SMA, whereas GFP^+ fibroblasts clustering in fibrotic regions where the interstitium was thickened often expressed α-SMA but not OPN (Figure 6F). OPN^+ GFP^+ fibroblasts localized to places where alveolar structures still remained, but which appeared to be undergoing remodeling to form fibrotic regions (Figure 6F). Taken together, these results suggest that activated fibroblasts, especially those located at the edges of fibrotic regions, secrete OPN into the alveolar air spaces, resulting in an accumulation of OPN on the luminal surfaces of alveolar walls.

Discussion

The development of novel therapeutic strategies against pulmonary fibrosis requires a better understanding of fibroblast activation in the context of disease. We investigated the changes that occur in lung tissue cell populations, including fibroblast populations, after the induction of fibrosis. Unexpectedly, the number of fibroblasts present in the lungs did not increase, even at the peak of fibrosis, probably because proliferation and apoptosis were promoted concurrently in the fibrotic condition. Activated GFP^+ fibroblasts possessed a characteristic phenotype consisting of enlarged cell size, increased intracellular organelle complexity, and up-regulation of genes involved in fibrogenesis. Of these genes, the OPN-encoding gene was the most highly up-regulated. OPN appeared to be secreted into alveolar spaces by activated fibroblasts located at the edges of fibrotic regions.

Fibrotic regions are considered to develop as a consequence of fibroblast migration, proliferation, and subsequent accumulation. Some *in vitro* studies suggest that activated fibroblasts acquire increased proliferative capacity.[25,26,43] In addition, fibrosis and wound healing models have shown expansion of myofibroblasts *in vivo*.[44,45] On the other hand, fibroblast proliferation has been shown to be inhibited by polymerized collagen,[46] suggesting that proliferative regulation of fibroblasts *in vivo* may depend on the microenvironment. In our model, we observed BrdU uptake and clustering by GFP^+ fibroblasts. Although there is a possibility that repair of DNA damage could contribute in part to BrdU uptake, the increase in proliferative cells observed in Fucci mice is consistent with BrdU uptake by proliferating fibroblasts.

Comprehensive gene expression analysis revealed an up-regulation of proliferative genes but not apoptotic genes, whereas an increase of apoptotic fibroblasts was detected by flow cytometry. This difference may have arisen because SAGE was performed at day 14, rather than

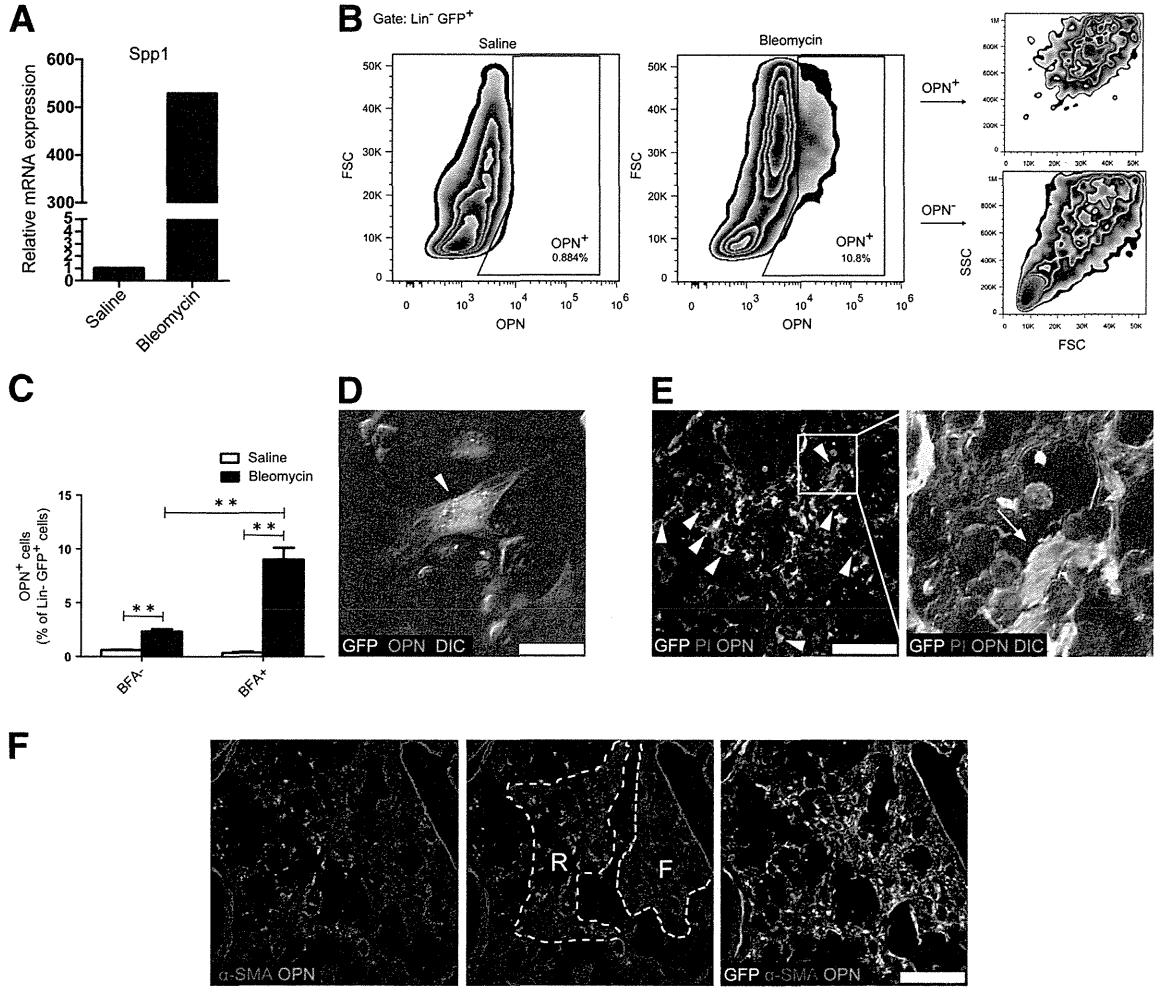

Figure 6 OPN is an activation marker of fibroblasts. **A:** mRNA isolated from sorted Lin$^-$ GFP$^+$ lung fibroblasts at 14 days after saline or bleomycin was analyzed by qPCR for *Spp1*. Template cDNA was pooled from the cells of three mice per group. **B:** Lung cells from Col1a2-GFP mice at 14 days after saline or bleomycin administration were cultured with BFA for 6 hours before staining for lineage markers and OPN (**left**). OPN$^+$ and OPN$^-$ Lin$^-$ GFP$^+$ fibroblasts from bleomycin-treated mice were plotted as FSC versus SSC (**right**). **C:** After 6 hour-culture of lung cells from saline or bleomycin-treated mice (day 14) with or without BFA, the proportion of Lin$^-$ GFP$^+$ cells that were OPN$^+$ was measured by flow cytometry. Data represent means ± SEM ($n = 4$). $^{**}P < 0.01$. **D:** Analysis by confocal microscopy of lung cells from Col1a2-GFP mice at 14 days after bleomycin administration. Cells were cultured *in vitro* with BFA for 6 hours before staining for OPN (red). OPN$^+$ GFP$^+$ cells are indicated by an **arrowhead**. **E:** Whole lungs from Col1a2-GFP mice at 14 days after bleomycin administration were cultured for 6 hours with BFA before sections were prepared and stained for OPN (red) and PI (blue). OPN$^+$ GFP$^+$ cells are indicated by **arrowheads** (**left**). The **boxed** region is shown at higher magnification at the **right**, highlighting an OPN$^+$ GFP$^+$ fibroblast (**arrow**) in an epithelium-denuded alveolus. **F:** Representative lung section from a Col1a2-GFP mouse at 14 days after bleomycin treatment, stained for α-SMA (blue) and OPN (red). Scale bars: 25 μm (**D**); 100 μm (**E**); 200 μm (**F**). F, fibrotic region; R, site of remodeling.

at day 7, when the peak of fibroblast apoptosis was observed. Also, because the proportion of apoptotic fibroblasts was very low (approximately 2%), the gene expression of apoptotic fibroblasts might have been negated by that of nonapoptotic fibroblasts. In such a case, the expansion of the population of GFP$^+$ fibroblasts revealed by their BrdU uptake might not have been sufficient to surpass the rate of cell death by apoptosis. Furthermore, long-term BrdU-uptake experiments revealed that fibroblasts can form fibrotic clusters without massive proliferation. These findings suggest that an absolute increase in fibroblast numbers is not necessarily critical to the pathogenesis of pulmonary fibrosis. Rather, it is fibroblast accumulation in clusters resulting from cell migration that is likely to be most important to the progression of fibrogenesis.

Immunohistochemical examination of fibrotic lungs revealed a massive increase in the number of GFP$^+$ fibroblast clusters in fibrotic regions. However, we do not believe that the increased density of GFP$^+$ fibroblasts that was observed with immunohistochemistry contradicts the flow-cytometric data showing that GFP$^+$ fibroblast numbers did not increase after bleomycin treatment. First, determining the proliferation of lung fibroblasts by histology is difficult, because fibrotic lung sections are filled with stroma (unlike normal lung sections, in which most of the area is made up of alveolar air spaces). Quantification of changes in tissue cell populations by flow cytometry after complete

digestion of whole lungs avoids such limitations. Second, in epithelium-denuded alveoli, fibroblasts encroach on the alveolar air space and there they secrete ECM components, resulting in coalescence of the alveolar walls.[47,48] Thus, the GFP^+ clusters observed in fibrotic regions are likely to be the result of fibroblast migration from surrounding alveolar walls into the alveolar air spaces. The up-regulation of genes associated with cell migration in GFP^+ fibroblasts supports this theory.

With the present study, we have identified OPN as an activation marker of lung fibroblasts during fibrosis. OPN is a matricellular protein that is implicated in various diseases, but that plays a different functional role from classical ECM proteins such as collagen or fibronectin.[49] Mori et al[50] found that knockdown of OPN decreased granulation tissue formation and scarring after skin injuries. Macrophage or mast cell-derived platelet-derived growth factor (PDGF) at the site of inflammation induced OPN expression in skin fibroblasts. Lenga et al[51] demonstrated that OPN is required for myofibroblast differentiation and activity in cardiac and skin fibroblasts. Macrophages, T cells, and epithelial cells are known sources of OPN in lung fibrosis. Although it has been reported previously that IL-1β induces OPN expression in lung fibroblasts *in vitro*,[52] the present study provides clear *in vivo* confirmation of OPN expression in lung fibroblasts during bleomycin-induced fibrosis. Other studies have suggested that epithelial cells, rather than fibroblasts, are the tissue cell source of OPN in pulmonary fibrosis.[35,42] A possible explanation for this discrepancy is that we treated the cells with BFA, and detection of the OPN protein in GFP^+ fibroblasts was greatly enhanced after BFA treatment (Figure 6C). Nevertheless, the relative contribution of various tissue cell populations, including fibroblasts, as sources of OPN in pulmonary fibrosis remains to be determined.

The finding that the OPN gene *Spp1* was highly up-regulated in GFP^+ fibroblasts after bleomycin treatment strongly suggests that OPN is involved in the pathogenesis of bleomycin-induced fibrosis. Previous studies have demonstrated that OPN enhances migration, invasion, and proliferation of lung fibroblasts.[35,53] Because OPN was abundant in alveolar air spaces, especially those near fibrotic regions, we suspect the involvement of OPN in the process of fibroblast migration to alveolar air spaces and in the formation of fibrotic foci through the coalescence of alveolar walls with ECM. In OPN-null mice, altered formation of fibrotic regions is observed, characterized by dilated distal air spaces.[42] Because the OPN gene *SPP1* is also one of the most highly up-regulated genes in human idiopathic pulmonary fibrosis,[35] understanding the role and mechanism action of OPN in the pathogenesis of fibrosis is likely to contribute to the development of novel therapies for this disease.

The comprehensive gene expression profile of freshly isolated fibroblasts suggested that activated fibroblasts became proliferative, resistant to cell death, mobile, and invasive. GO term enrichment demonstrated a role for these cells in ECM depositions, and flow cytometry and immunohistochemistry revealed expression of α-SMA in some GFP^+ fibroblasts. These findings suggest that, after bleomycin treatment, some GFP^+ resident fibroblasts differentiate into myofibroblasts and play a critical role in fibrogenesis. However, because the possibility cannot be excluded that other cell types such as epithelial cells acquire GFP expression and a fibroblast phenotype after bleomycin treatment, the findings in the present study should be confirmed by strict lineage tracing of fibroblasts. We demonstrated that GFP^+ fibroblasts in the lungs were not supplied from the circulation. In a study using the same Col1a2-GFP reporter mice, Higashiyama et al[54] found that limited but significant number of $CD45^+$ collagen type I–positive cells were recruited to skin in bleomycin-induced skin fibrosis. A possible explanation for the discrepancy between the present study and previous studies of fibrocytes is that we used parabiosis instead of bone marrow transplantation. Our present results clearly showed that circulating mesenchymal cells do not contribute significantly to fibroblast population in the lungs, and most of the fibroblasts in fibrotic regions are residential.

Interestingly, the localization of α-SMA–expressing fibroblasts and OPN-expressing fibroblasts differed. α-SMA–expressing fibroblasts were prominent within fibroblast clusters, whereas OPN-expressing fibroblasts were commonly located at the boundary of fibrotic regions and alveolar spaces. Thus, OPN expression and α-SMA expression may represent different stages of fibrogenesis. Currently, most fibrosis studies rely on α-SMA as a unique marker for myofibroblasts, based on the premise that myofibroblasts are the most important cell population in fibrogenesis. Given the various biological functions that OPN contributes to fibrogenesis, our findings suggest that OPN^+ collagen type I-producing fibroblasts represent a novel population of fibroblasts that play an important role in fibrogenesis, a role distinct from that of myofibroblasts.

In conclusion, we have revealed *in vivo* properties of fibroblasts during bleomycin-induced pulmonary fibrosis, showing their profibrotic signatures without changes in number. From the gene expression profile, the gene encoding OPN was identified as the most highly expressed gene in fibroblasts, with distinct localizations that are different from those of myofibroblasts, suggesting potential use of OPN as a novel activation marker of fibroblasts. Taken together, these findings provide useful insights toward further elucidation of the cellular and molecular mechanisms of pulmonary fibrosis.

Acknowledgments

We thank Dr. Atsushi Miyawaki and the RIKEN Bio-Resource Center cell bank for supplying FucciG1-#639 and FucciS/G2/M-#474 mice.

Supplemental Data

Supplemental material for this article can be found at *http://dx.doi.org/10.1016/j.ajpath.2013.06.005*.

References

1. Wynn TA, Ramalingam TR: Mechanisms of fibrosis: therapeutic translation for fibrotic disease. Nat Med 2012, 18:1028–1040
2. King TE Jr, Pardo A, Selman M: Idiopathic pulmonary fibrosis. Lancet 2011, 378:1949–1961
3. Wynn TA: Cellular and molecular mechanisms of fibrosis. J Pathol 2008, 214:199–210
4. Hinz B, Phan SH, Thannickal VJ, Galli A, Bochaton-Piallat ML, Gabbiani G: The myofibroblast. Am J Pathol 2007, 170:1807–1816
5. Wynn TA: Integrating mechanisms of pulmonary fibrosis. J Exp Med 2011, 208:1339–1350
6. Noble PW, Barkauskas CE, Jiang D: Pulmonary fibrosis: patterns and perpetrators. J Clin Invest 2012, 122:2756–2762
7. Kim KK, Wei Y, Szekeres C, Kugler MC, Wolters PJ, Hill ML, Frank JA, Brumwell AN, Wheeler SE, Kreidberg JA, Chapman HA: Epithelial cell alpha3beta1 integrin links beta-catenin and Smad signaling to promote myofibroblast formation and pulmonary fibrosis. J Clin Invest 2009, 119:213–224
8. Tanjore H, Xu XC, Polosukhin VV, Degryse AL, Li B, Han W, Sherrill TP, Plieth D, Neilson EG, Blackwell TS, Lawson WE: Contribution of epithelial-derived fibroblasts to bleomycin-induced lung fibrosis. Am J Respir Crit Care Med 2009, 180:657–665
9. Hoyles RK, Derrett-Smith EC, Khan K, Shiwen X, Howat SL, Wells AU, Abraham DJ, Denton CP: An essential role for resident fibroblasts in experimental lung fibrosis is defined by lineage-specific deletion of high-affinity type II transforming growth factor receptor. Am J Respir Crit Care Med 2010, 183:249–261
10. Rock JR, Barkauskas CE, Cronce MJ, Xue Y, Harris JR, Liang J, Noble PW, Hogan BLM: Multiple stromal populations contribute to pulmonary fibrosis without evidence for epithelial to mesenchymal transition. Proc Natl Acad Sci USA 2011, 108:E1475–E1483
11. Lin SL, Kisseleva T, Brenner DA, Duffield JS: Pericytes and perivascular fibroblasts are the primary source of collagen-producing cells in obstructive fibrosis of the kidney. Am J Pathol 2008, 173: 1617–1627
12. Göritz C, Dias DO, Tomilin N, Barbacid M, Shupliakov O, Frisén J: A pericyte origin of spinal cord scar tissue. Science 2011, 333: 238–242
13. Herzog EL, Brody AR, Colby TV, Mason R, Williams MC: Knowns and unknowns of the alveolus. Proc Am Thorac Soc 2008, 5:778–782
14. Kunz-Schughart LA, Wenninger S, Neumeier T, Seidl P, Knuechel R: Three-dimensional tissue structure affects sensitivity of fibroblasts to TGF-beta 1. Am J Physiol Cell Physiol 2003, 284:C209–C219
15. De Val S, Ponticos M, Antoniv TT, Wells DJ, Abraham D, Partridge T, Bou-Gharios G: Identification of the key regions within the mouse pro-alpha 2(I) collagen gene far-upstream enhancer. J Biol Chem 2001, 277:9286–9292
16. Higashiyama R, Moro T, Nakao S, Mikami K, Fukumitsu H, Ueda Y, Ikeda K, Adachi E, Bou-Gharios G, Okazaki I, Inagaki Y: Negligible contribution of bone marrow-derived cells to collagen production during hepatic fibrogenesis in mice. Gastroenterology 2009, 137: 1459–1466
17. Tomura M, Mori YS, Watanabe R, Tanaka M, Miyawaki A, Kanagawa O: Time-lapse observation of cellular function with fluorescent probe reveals novel CTL-target cell interactions. Int Immunol 2009, 21:1145–1150
18. Foster WM, Walters DM, Longphre M, Macri K, Miller LM: Methodology for the measurement of mucociliary function in the mouse by scintigraphy. J Appl Physiol 2001, 90:1111–1117
19. Shimbori C, Shiota N, Okunishi H: Involvement of leukotrienes in the pathogenesis of silica-induced pulmonary fibrosis in mice [Erratum appeared in Exp Lung Res 2010, 36:440]. Exp Lung Res 2010, 36: 292–301
20. Fujita M, Shannon JM, Irvin CG, Fagan KA, Cool C, Augustin A, Mason RJ: Overexpression of tumor necrosis factor-alpha produces an increase in lung volumes and pulmonary hypertension. Am J Physiol Lung Cell Mol Physiol 2001, 280:L39–L49
21. Huang DW, Sherman BT, Lempicki RA: Systematic and integrative analysis of large gene lists using DAVID bioinformatics resources. Nat Protoc 2008, 4:44–57
22. Kapanci Y, Ribaux C, Chaponnier C, Gabbiani G: Cytoskeletal features of alveolar myofibroblasts and pericytes in normal human and rat lung. J Histochem Cytochem 1992, 40:1955–1963
23. Fukuda Y, Ferrans VJ, Schoenberger CI, Rennard SI, Crystal RG: Patterns of pulmonary structural remodeling after experimental paraquat toxicity. The morphogenesis of intraalveolar fibrosis. Am J Pathol 1985, 118:452–475
24. Kawamoto M, Fukuda Y: Cell proliferation during the process of bleomycin-induced pulmonary fibrosis in rats. Acta Pathol Jpn 1990, 40:227–238
25. Moseley PL, Hemken C, Hunninghake GW: Augmentation of fibroblast proliferation by bleomycin. J Clin Invest 1986, 78:1150–1154
26. Mio T, Nagai S, Kitaichi M, Kawatani A, Izumi T: Proliferative characteristics of fibroblast lines derived from open lung biopsy specimens of patients with IPF (UIP). Chest 1992, 102:832–837
27. Messier EM, Mason RJ, Kosmider B: Efficient and rapid isolation and purification of mouse alveolar type II epithelial cells. Exp Lung Res 2012, 38:363–373
28. Mouratis MA, Aidinis V: Modeling pulmonary fibrosis with bleomycin. Curr Opin Pulm Med 2011, 17:355–361
29. Zhang K, Rekhter MD, Gordon D, Phan SH: Myofibroblasts and their role in lung collagen gene expression during pulmonary fibrosis. A combined immunohistochemical and in situ hybridization study. Am J Pathol 1994, 145:114–125
30. Takemoto K: Spatio-temporal activation of caspase revealed by indicator that is insensitive to environmental effects. J Cell Biol 2003, 160:235–243
31. Nagai T, Miyawaki A: A high-throughput method for development of FRET-based indicators for proteolysis. Biochem Biophys Res Commun 2004, 319:72–77
32. Sakaue-Sawano A, Kurokawa H, Morimura T, Hanyu A, Hama H, Osawa H, Kashiwagi S, Fukami K, Miyata T, Miyoshi H, Imamura T, Ogawa M, Masai H, Miyawaki A: Visualizing spatiotemporal dynamics of multicellular cell-cycle progression. Cell 2008, 132:487–498
33. Phillips RJ, Burdick MD, Hong K, Lutz MA, Murray LA, Xue YY, Belperio JA, Keane MP, Strieter RM: Circulating fibrocytes traffic to the lungs in response to CXCL12 and mediate fibrosis. J Clin Invest 2004, 114:438–446
34. Hashimoto N: Bone marrow-derived progenitor cells in pulmonary fibrosis. J Clin Invest 2004, 113:243–252
35. Pardo A, Gibson K, Cisneros J, Richards TJ, Yang Y, Becerril C, Yousem S, Herrera I, Ruiz V, Selman M, Kaminski N: Up-regulation and profibrotic role of osteopontin in human idiopathic pulmonary fibrosis. PLoS Med 2005, 2:e251
36. Kaminski N, Allard JD, Pittet JF, Zuo F, Griffiths MJ, Morris D, Huang X, Sheppard D, Heller RA: Global analysis of gene expression in pulmonary fibrosis reveals distinct programs regulating lung inflammation and fibrosis. Proc Natl Acad Sci USA 2000, 97: 1778–1783
37. Kass DJ, Yu G, Loh KS, Savir A, Borczuk A, Kahloon R, Juan-Guardela B, Deiuliis G, Tedrow J, Choi J, Richards T, Kaminski N, Greenberg SM: Cytokine-like factor 1 gene expression is enriched in idiopathic pulmonary fibrosis and drives the accumulation of CD4+ T cells in murine lungs. Am J Pathol 2012, 180:1963–1978
38. Oikonomou N, Thanasopoulou A, Tzouvelekis A, Harokopos V, Paparountas T, Nikitopoulou I, Witke W, Karameris A, Kotanidou A,

Bouros D, Aidinis V: Gelsolin expression is necessary for the development of modelled pulmonary inflammation and fibrosis. Thorax 2009, 64:467–475
39. Zhou Y, Koli K, Hagood JS, Miao M, Mavalli M, Rifkin DB, Murphy-Ullrich JE: Latent transforming growth factor-β-binding protein-4 regulates transforming growth factor-β1 bioavailability for activation by fibrogenic lung fibroblasts in response to bleomycin. Am J Pathol 2009, 174:21–33
40. Ishii Y: Gefitinib prevents bleomycin-induced lung fibrosis in mice. Am J Respir Crit Care Med 2006, 174:550–556
41. Wilson MS, Madala SK, Ramalingam TR, Gochuico BR, Rosas IO, Cheever AW, Wynn TA: Bleomycin and IL-1-mediated pulmonary fibrosis is IL-17A dependent. J Exp Med 2010, 207:535–552
42. Berman JS: Altered bleomycin-induced lung fibrosis in osteopontin-deficient mice. Am J Physiol Lung Cell Mol Physiol 2004, 286: L1311–L1318
43. Ramos C, Montaño M, García-Alvarez J, Ruiz V, Uhal BD, Selman M, Pardo A: Fibroblasts from idiopathic pulmonary fibrosis and normal lungs differ in growth rate, apoptosis, and tissue inhibitor of metalloproteinases expression. Am J Respir Cell Mol Biol 2001, 24:591–598
44. Humphreys BD, Lin SL, Kobayashi A, Hudson TE, Nowlin BT, Bonventre JV, Valerius MT, McMahon AP, Duffield JS: Fate tracing reveals the pericyte and not epithelial origin of myofibroblasts in kidney fibrosis. Am J Pathol 2010, 176:85–97
45. Virag JI, Murry CE: Myofibroblast and endothelial cell proliferation during murine myocardial infarct repair. Am J Pathol 2003, 163: 2433–2440
46. Xia H, Nho R, Kleidon J, Kahm J, Henke CA: Polymerized collagen inhibits fibroblast proliferation via a mechanism involving the formation of a beta1 integrin-protein phosphatase 2A-tuberous sclerosis complex 2 complex that suppresses S6K1 activity. J Biol Chem 2008, 283:20350–20360
47. Noble PW: Back to the future: historical perspective on the pathogenesis of idiopathic pulmonary fibrosis. Am J Respir Cell Mol Biol 2005, 33:113–120
48. Myers J, Katzenstein A: Epithelial necrosis and alveolar collapse in the pathogenesis of usual interstitial pneumonia. Chest 1988, 94: 1309–1311
49. Uede T: Osteopontin, intrinsic tissue regulator of intractable inflammatory diseases. Pathol Int 2011, 61:265–280
50. Mori R, Shaw TJ, Martin P: Molecular mechanisms linking wound inflammation and fibrosis: knockdown of osteopontin leads to rapid repair and reduced scarring. J Exp Med 2008, 205:43–51
51. Lenga Y, Koh A, Perera AS, McCulloch CA, Sodek J, Zohar R: Osteopontin expression is required for myofibroblast differentiation. Circ Res 2008, 102:319–327
52. Serlin DM, Kuang PP, Subramanian M, O'Regan A, Li X, Berman JS, Goldstein RH: Interleukin-1β induces osteopontin expression in pulmonary fibroblasts. J Cell Biochem 2006, 97:519–529
53. Anwar A, Li M, Frid MG, Kumar B, Gerasimovskaya EV, Riddle SR, McKeon BA, Thukaram R, Meyrick BO, Fini MA, Stenmark KR: Osteopontin is an endogenous modulator of the constitutively activated phenotype of pulmonary adventitial fibroblasts in hypoxic pulmonary hypertension. Am J Physiol Lung Cell Mol Physiol 2012, 303:L1–L11
54. Higashiyama R, Nakao S, Shibusawa Y, Ishikawa O, Moro T, Mikami K, Fukumitsu H, Ueda Y, Minakawa K, Tabata Y, Bou-Gharios G, Inagaki Y: Differential contribution of dermal resident and bone marrow–derived cells to collagen production during wound healing and fibrogenesis in mice. J Invest Dermatol 2011, 131: 529–536

最近の研究

マウス皮膚創傷治癒モデルにおける筋膜由来線維芽細胞と希少コラーゲンのはたらき

住吉秀明*
稲垣豊**

1．はじめに

コラーゲンは動物の細胞外マトリックス（Extracellular Matrix：以下ECM）の主成分を成す線維性構造タンパク質である．多細胞生物はECMの存在なしに成立せず，私はその重要性を表現する際にレンガ建築のレンガ（細胞）とセメント（ECM）に例えたりしている．コラーゲンは動物性タンパク質の3割を占める最も豊富な成分であるとともに，グリシン，プロリンの含有量が高く，自身のコラーゲンを合成するためにおいても良質の動物性タンパク質である．そのイメージは健康食品や美容，アンチエイジングの話題を中心とした健康に良い善玉として一般的にもよく浸透している．それに対し，我々は医学部の研究テーマにおいて肝硬変をはじめとする組織・臓器線維症を治療する研究を行っており，そこではコラーゲンは線維化を引き起こす悪玉として，如何に合成・蓄積されないようにするかを研究している．コラーゲンの総量は精妙に調節されなければならないが，慢性炎症等の病的要因により生合成と分解のバランスが崩れて過多に蓄積することにより，組織・臓器の機能を損なうのが線維症の実体である．コラーゲンはどの組織にも存在するため，線維化病変は肺線維症，腎硬化症，ケロイドの形成，手術後の癒着など，多領域にわたって重篤な疾患が存在し，これから解決されなければならない医療上の課題となっている．

本稿では傷病により誘導されたコラーゲンが如何にして構築・形成されていくかの過程をリアルタイムで観察する目的で，マウス皮膚創傷治癒をモデルとし，活性化線維芽細胞の動員，発現誘導されるコラーゲン遺伝子群の型別解析，コラーゲン線維束の形成過程を分子会合レベルで解析した例を示す．それらの結果，動員される線維芽細胞は真皮のものではなく，筋膜由来の静止線維細胞が活性化して動員されたもので，形成されるコラーゲン線維の性質も異なるということ，この細胞は希少コラーゲン分子種であるV型コラーゲンα3鎖（以下α3（V）と表記）を特異的に発現すること，このα3（V）はコラーゲン線維の会合・集束を阻害することで，その過剰形成を自ら抑制し，また皮膚組織と筋膜組織の癒着の防止に働いていることが新たに見出された．コラーゲンは多細胞組織に必要とされる生育環境の土台であり，線維の産生は細胞が生育環境を造りだそうとする自己防衛反応であるが，これは線維構築を制御し，安定終息させる生体側の仕組みであると思われ，その機序の解明が期待される．この稿は本会誌の中で，少し側面の異なる話となるが読者にとって，新たな興味となれれば幸いである．

2．実験の背景

コラーゲンは結合組織の支持体として働いているが，同時にそれは単なる支持体ではなく，他のECM分子と共に細胞の外部生育環境を構成し“細胞のゆりかご”として機能している．細胞に適した“足場”を提供し，また情報伝達の媒体となり，細胞に適する居場所や方向性の情報を与え，細胞と共に組織の形態を決定していく．このような能動的な役割を有しており，必ずしもセメントのような“接着させる物質”では無い．本来，細胞とECMは組織形態維持と機能発現に不可欠な要素であるが，その比率と正常な配位関係が失われれば，お互い足を引っ張り合う様に機能不全に陥る．特に肝臓は大きな再生能力を有しているにもかかわらず，肝硬変になると線維化によって肝再生が障害される．肝線維症の治療と肝細胞の再生医療は同じ事象の表裏であり，抗線維化治療法の開発の持つ意味は大き

*Hideaki Sumiyoshi：東海大学医学部再生医療科学，同総合医学研究所特任講師，**Yutaka Inagaki：東海大学医学部再生医療科学，同総合医学研究所教授，〒259-1193 神奈川県伊勢原市下糟屋143，TEL 0463(93)1121，内線3068

い．コラーゲンは如何にして蓄積されるのだろうか．コラーゲンは29種の型に分類されるスーパーファミリーを形成しており，46のα鎖遺伝子が確認されているが，組織線維化に関係するのは線維性コラーゲンであるⅠ，Ⅲ，Ⅴ型コラーゲンであり，その中でも線維を構築する過程で果たす役割が異なっている[1]．Ⅰ型は最も多い成分で組織線維症の“主犯”として捉えられている．図1に一般的な線維性コラーゲンの各α鎖と呼ばれる遺伝子が，コラーゲンドメインであるGly-X-Yモチーフにより3重らせん構造のトリマー分子となり，それらが細胞外でプロセスを受けた後に自己会合して束を形成することで“コラーゲン線維”が形成されていくという過程を示す．正常組織のコラーゲン線維を電子顕微鏡で観察すると，真皮や腱の様に，直径100nmを超える線維が規則的に張り巡らされている組織もあれば，直径10数nm程の細かい線維が分岐して緩く敷き詰められ，細胞の生育環境を形成している組織もあり，バリエーションに富んでいる．これらの細胞外環境の違いはコラーゲンの線維束の組まれ方によってもたらされ，当該組織の機能と密接に関係している．太い線維でも細いものでも主成分はⅠ型コラーゲンであるが，Ⅲ型とⅤ型は形成途中の細いコラーゲンに，より多く含まれる．特にⅤ型α1鎖はN末にテロペプチドと呼ばれる特徴的な非コラーゲン領域を有しており（図1C），立体的な制約からⅤ型コラーゲンはコラーゲン線維束の外周部分に配置され，線維の隙間からN末ドメインを突き出す形態をとる（図1D）．このためⅤ型コラーゲン含量が増すと線維径が細くなるとされる．このN末領域の役割は解明されていないが，他のECM分子と相互作用しながらコラーゲン線維の径を調節すると考えられている[2]．またⅤ型α1鎖のKOマウスは，全くコラーゲン線維を形成できず致死となり，線維の形成初期にⅤ型コラーゲンが芯を形成する役割があるとみられる[3]など，線維束の形成機構について重要なヒントを握っているものと考えられる．

我々は線維化におけるコラーゲン線維束の形成と蓄積の過程を追跡したいと考え，マウスの背部皮膚に穴を空け，その欠損部を埋める過程において各種コラーゲン遺伝子の動き，線維芽細胞の動員，コラーゲン線維束の電子顕微鏡レベルでの形態形成を観察する実験を行なった．

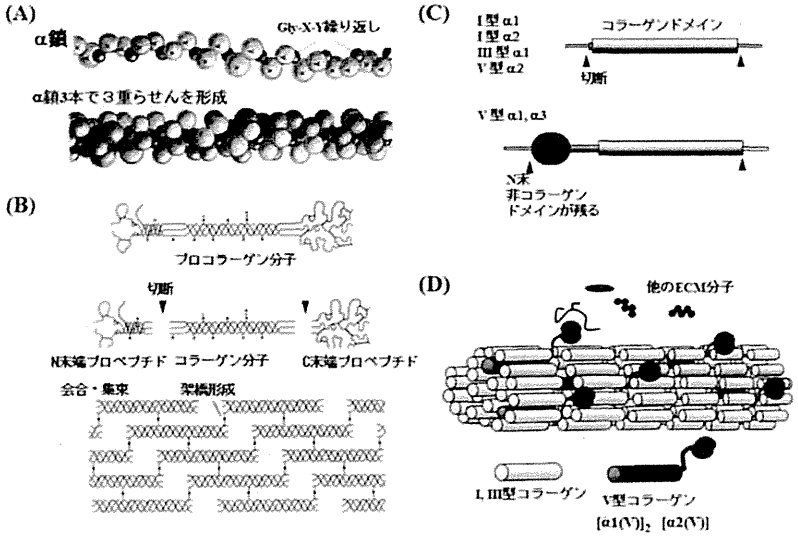

図1　線維性コラーゲンの構造と線維束の構築

（A）コラーゲンドメインのアミノ酸一次構造，Gly-X-Y繰り返し構造と，小さいグリシン残基が綾りあわせの中心となり3重らせん構造を形成するモデルを示す．（Bruce, A. et al.：Molecular Biology of the Cell, Garland Science, 2007より出典）
（B）線維性コラーゲンの会合．分泌直後はプロコラーゲンとしてN，C末のプロペプチドを持つが，細胞外でプロペプチドが切断を受け，成熟コラーゲン分子となり，会合体を形成する．この束が電子顕微鏡で観察されるコラーゲン線維である．（大塚吉兵衛，安孫子宣光著：医歯薬系学生のためのビジュアル生化学・分子生物学（改訂第3版）日本医事新報社，2008より出典）
（C）Ⅰ型，Ⅲ型，Ⅴ型コラーゲンの構造の違い．Ⅰ型，Ⅲ型，Ⅴ型α2鎖はプロペプチドを除くと純粋な3重らせん構造が残るが，Ⅴ型α1鎖とα3鎖はプロペプチド以外にN末に残る非コラーゲンドメイン，テロペプチドを有する構造をしている．
（D）線維性コラーゲンの会合模式図．Ⅰ型，Ⅲ型を基本としてコラーゲンの束が形成される．Ⅴ型コラーゲンはN末のテロペプチドの為，線維の外周部に配置し，他のECM分子とのインタラクションを通じて線維の構築を調節するとされている．
(Lynsenmayer, T. F. et al, J. Cell Biol 1993.（文献2）より改変)

3．実験結果１：各種コラーゲン遺伝子の発現と治癒後のコラーゲン組織

マウスの創傷治癒による創部の再生は，短期間でコラーゲンの新生と線維構築過程を観察する最良のモデルである．マウスの背部皮膚に直径６㎜の全層欠損創を形成し，各種コラーゲン遺伝子の活性化と発現局在を *In situ* hybridization を用いて調べた（図２）．ここで示すコラーゲン遺伝子（Ⅰ型α１，Ⅲ型α１，Ⅴ型α１，α３）は，創傷後４日後から新生肉芽組織を中心に，ほぼ同時に発現し始めた．中でもⅤ型コラーゲンは創傷前には殆ど発現が見られなかったが，創傷

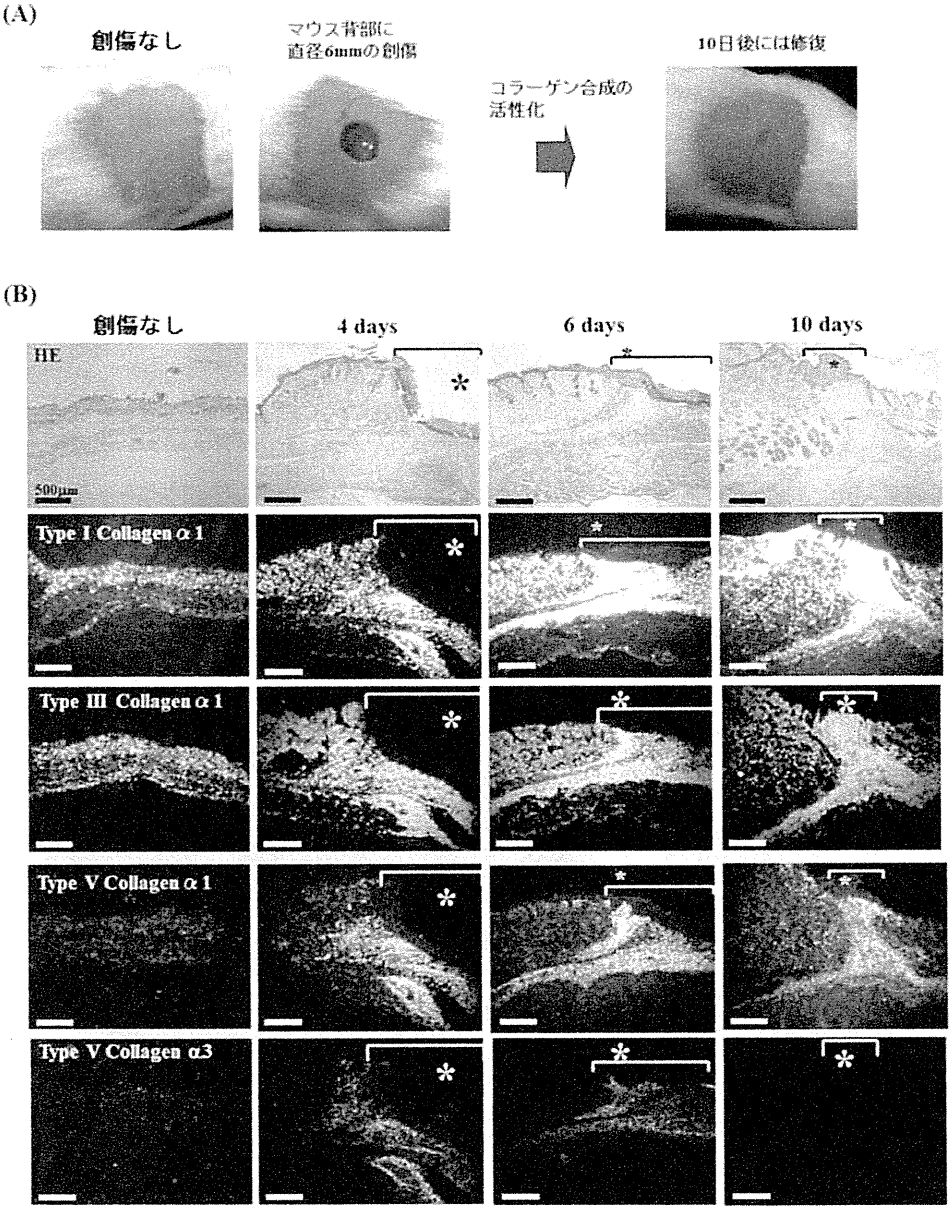

図２　皮膚創傷治癒における各種コラーゲン遺伝子の発現パターン

（A）マウス背部に６㎜の皮膚全層欠損創を形成した外観．10日程で傷は修復される．
（B）創傷部の組織像．左から創傷なし，創傷後４日，６日，10日後の組織像．＊が創傷部分を示す．写真上段からHE染色像，Ⅰ型α１鎖の *In situ* hybridization，同じくⅢ型α１鎖，Ⅴ型α１鎖，Ⅴ型α３鎖の *In situ* を示している．白く見えるシグナルが，各コラーゲン遺伝子の mRNA 発現に対応する．Ⅴ型コラーゲンの方が創部に，より特異的に発現しているのが分かる．Bar は500μm．
（Sumiyoshi, H. et al, Connect. Tissue Res. 2012.（文献４）より改変）

部の領域で急激に発現量が増しており，Ⅰ型より明瞭なコントラストを成していた．この事からも形成中のコラーゲンに，より多くのⅤ型コラーゲンが含まれていることが確認できた．この実験は線維形成に関わるコラーゲン分子種を網羅的に探していく事を目的としており，本来皮膚には発現しないとされるコラーゲン種（Ⅱ型α1，XI型α1ともに陰性）もまた解析を試みた．その中から胎児期の臍帯や羊膜に発現しているが，成体の組織中に通常見られないα3（Ⅴ）が，皮膚創傷治癒事例でのコラーゲン線維形成初期にのみ特異的に発現してくることが見出された．このことについては改めて後述したい．

電子顕微鏡で新生コラーゲンの構築過程を観察すると，創傷部位には細くて方向性がばらばらの，分岐のあるコラーゲン線維①と，太くて規則的に並行する分岐のないコラーゲン線維② が存在し，（図3 A）線維化が進むにつれ，太い線維の密度が増していった．しかし創傷部の新生コラーゲンは太いものでも，50nm程であり，真皮コラーゲン線維（100nm以上）の半分である．またコラーゲンの形態にも明らかな違いがあり，真皮コラーゲンはきれいな流紋を示し，多方向に組まれ，表面も滑らかである一方，新生コラーゲンに由来する傷痕部は平板で層状に配列しており表面には真皮にない粗さがあった．線維芽細胞の形態も異なり，真皮線維芽細胞は星形を示すのに対し，傷痕部の線維芽細胞は横長である．このように創傷部に再建された組織は正規のものと異なる構造を持っていた（図3 B）．そのためか傷痕は1年を経過しても明瞭に見分けることが出来た．この線維形態は皮下筋膜の結合組織にみられるコラーゲンの構造と類似している．ここで，創傷部位のHE染色像と *In situ* hybridizationの観察像を再度見直してみると，コラーゲンを強く発現している線維芽細胞の領域は真皮からではなく，皮下と筋膜との境界部結合組織から流れて来るようなパターンが見られる．更に後になって特徴的な発現パターンを示していたコラーゲンα3（Ⅴ）の発現は筋膜由来細胞に特異的であることが示された．

これらの筋膜に存在する細胞はマイルドなコラゲナーゼ処理にて，ほぼ均一な細胞群として単離することが出来た．これらは，細胞骨格に乏しく，多数の空胞をもった，正常筋膜内に多数観察される細胞であるが，これを培養下，血清で活性化したところ，創傷部にみられる充実した粗面小胞体を持ち，アクチンファイバーの発達した細胞に形態変化を起こし，線維産生細胞になることが確認できた（図4）．つまり，皮膚の創傷を埋めたのは本来の皮膚由来である真皮線維芽細胞ではなく，創傷という非常事態に際して活性化し，遊走・増殖してきた筋膜の細胞であり，埋められたコラーゲ

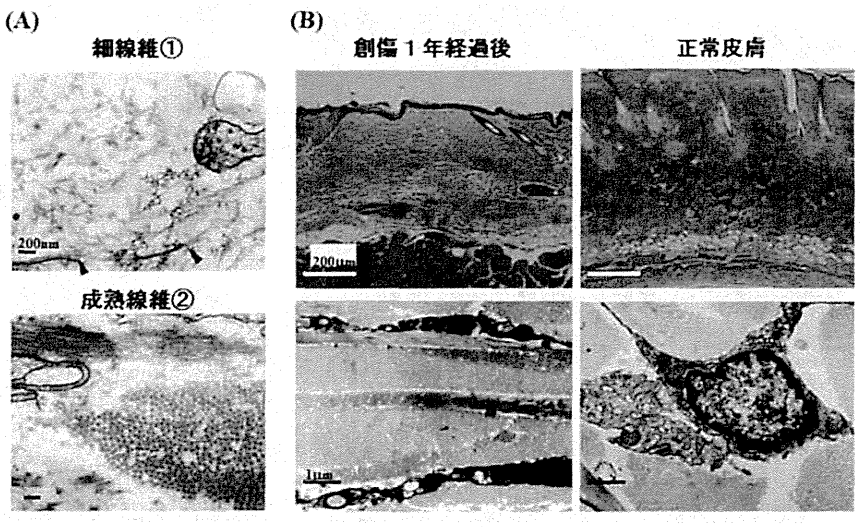

図3　新生コラーゲンにみられる，2種類のコラーゲン線維

(A) 細線維①は直径15nm程のばらついた形状の細い線維．会合・集束しつつある線維もみられる（矢頭）．成熟線維②は直径50nm程で方向も揃った形状を示す．Barは200nm.

(B) 左側：創傷1年後線維瘢痕組織，右側：正常皮膚組織．上段：マッソントリクローム染色．創傷後瘢痕のコラーゲン線維走行は平坦だが，正常真皮は流紋状を示す．Barは200μm．下段：同部位の電子顕微鏡像．創傷後瘢痕のコラーゲンは直径50nm程の水平方向の層構造で，線維芽細胞も横長の形態を示す．正常真皮は直径100nm以上の3次元に張り巡らされた線維で線維芽細胞は星形の形態を示す．Barは1μm.

（住吉秀明，稲垣豊：医学のあゆみ Vol. 244, No 6，医歯薬出版株式会社，2013より出典）

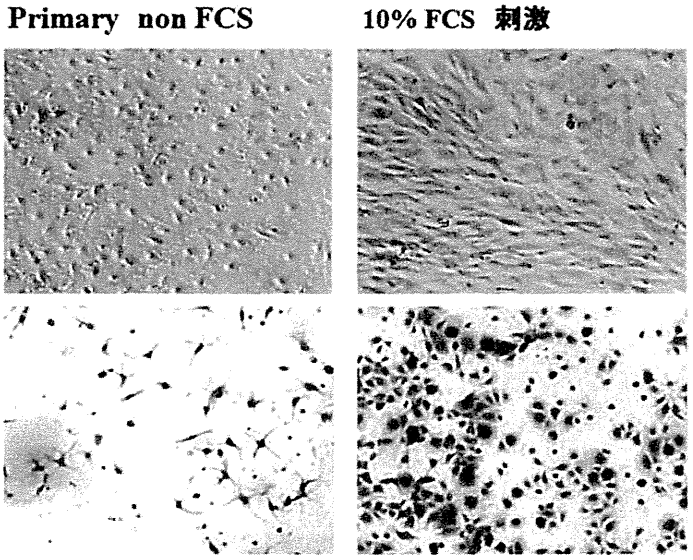

図4 筋膜細胞の初代培養と血清による活性化

左列：単離直後の筋膜細胞，無血清条件．右列：10%血清で刺激した後，継代した筋膜細胞．上段：位相差顕微鏡像．下段：クリスタルバイオレット染色像．単離した直後の筋膜細胞は長い触手をもち，血清なしでは増殖せず形態を保つが，血清を加えて活性化すると細胞は伸展し，活発な増殖を始める．

ンは異所性のリモデリングにより再生されたということが出来る．これらの細胞は静止状態では，ほとんどコラーゲンを産生しないが，刺激を受けると線維産生細胞となる前駆細胞と言えるものであり，肝線維化における星細胞の活性化機構にも通じるものとして興味深い．このことがどんな生体的な意味をもつのかを考察するに，一度出来上がった組織が損傷した際，本来の構成細胞をもって修復することは発生を逆行させる様に難しいことであり，むしろ修復屋といえる準万能細胞を各組織に配置しておいて対応する方が合目的であると考えることが出来る．そして，線維症とは線維産生細胞への活性化が持続するような要因が加わることによる創傷修復過程からの逸脱であると捉えられる．皮膚浅筋膜由来細胞は単離しやすく，線維産生細胞への形質転換モデル細胞として活性化を遮断する薬剤開発にも使えるのではないかと期待している．

4．実験結果2：創傷治癒過程におけるα3（V）鎖の発現について

ここで新たに見出された創傷部のα3（V）鎖の発現について述べる．α3（V）はV型コラーゲン遺伝子の一つであり，成体マウスの組織中にほとんど見られない希少なコラーゲン分子種である．以前から第三のV型コラーゲンα鎖があることが知られていたが，α3（V）遺伝子構造が明らかなったのは近年である[5]．通常のV型コラーゲンはα1鎖2本とα2鎖1本からなるヘテロトリマー［α1（V）］2［α2（V）］でありα3（V）は含まれていない（図1C，D）．α3（V）鎖はα1鎖，α2鎖と共同して［α1（V）］［α2（V）］［α3（V）］の3種ヘテロトリマーを形成し，単独で3重らせんを巻くことはない．α3（V）鎖を含むコラーゲン線維は通常のV型コラーゲンと，この3種トリマーが混在する形になる．α3鎖のN末にもテロペプチドが存在し，α1鎖のN末ドメインが酸性アミノ酸に富むのに対し，α3鎖のN末は塩基性アミノ酸が多く含まれ，全く異なる機能をもつと考えられる．この領域はヘパリン硫酸糖鎖結合ドメインが含まれ，良好な細胞接着性をもつ事が示されている[6]．α3（V）鎖は主に胎児期の臍帯，羊膜，筋膜，骨膜などに局在し，生後には見られなくなる[6]．

この特殊なコラーゲン種が創傷治癒過程に見出され，新生コラーゲンの構築に付与していること，また4日目と6日目に発現があり，10日目以後には，消失してしまう時期特異性があり，発現部位についても筋膜との境界部，真皮との境界部，表皮細胞との境界部等，境をなす部位により多くみられる部位特異性がみられた（図2）．面白いことに，これらのα3（V）鎖が多く発現する領域はコラーゲン線維の会合集束が抑制され，細線維が多く線維密度がルーズである傾向があり，特に皮下組織と筋膜の成すα3（V）鎖の豊富な境界部には剥離面が形成され，癒着が解消される現象が見られた．この剥離面を詳しくみると，末端の細胞

の底面に，α3（V）鎖を含む細線維のコラーゲンがびっしり付着し，その側には基底膜が形成されつつあること，その反対側の細胞面には絨毛状の突起が出現し，全くコラーゲン線維のない領域が成されているなどの，細胞に表裏の極性が生じている所見が観察された（**図5上左ⒶⒷ**），またα3（V）鎖の産生は筋膜（特に浅筋膜・上筋膜）細胞に特異的であり，筋より深部に及んだ創傷ではα3（V）鎖が減少し，その領域ではコラーゲンの束が早くまとまり，線維化がより早く進行する事（**図5上右**）と，癒着が起こりやすくなる事が観察された．

これを受け，α3（V）鎖が癒着を防止するメカニズムを分子レベルで解析するため，α3（V）鎖の特異的抗体を作製し，免疫電子顕微鏡解析を用いてコラーゲン線維上での分子局在を観察した．その結果，本分子はコラーゲン線維の束に取り込まれておらず，周囲にまとわり付く付着物様の物質中に存在している事が明らかとなった（**図5下左**）．この物質はα3（V）鎖のみでなく，周囲のECM成分を巻き込んでいると考えられたため，親和性が確認されているヘパラン硫酸糖鎖特異的抗体を併用した免疫二重電顕で解析したところ，分子レベルにおいてα3（V）とヘパラン硫酸糖鎖が共局在していることが示された（**図5下左**）．これらの観察結果から，V型コラーゲンはコラーゲンが線維として会合集束する際，線維束の外周に位置して線維を整形し，径を調整するとみられているが，α3（V）鎖が加わると，ヘパラン硫酸糖鎖を含む周囲のECM分子と強くインタラクションすることにより，集束の過程が阻害され，過度の線維化を抑制するものと考えられる（**図6**）．また，α3（V）鎖を含む細線維のコラーゲンマトリックスはヘパラン硫酸糖鎖を細胞接着レセプターとして有する細胞にちょうど良い足場を提供し，またそれが接着面特異的なサイトカインのシグナルを中継点となりうることで，細胞に極性の情報を与えるものと考察できる．

つまりα3（V）鎖は①コラーゲン線維の集束形成を抑制する（抗線維化効果），②細胞に足場を提供し極性を与える（細胞の生育環境・組織の構築）という大変有用な機能を有している．さらに，α3（V）鎖は微量成分にすぎないにも拘わらず線維の形態と機能に変化を与え，コラーゲン自らによる線維化のコントロール，組織再構築を行なう実働分子として，その応用が大変期待される．

5．おわりに

肝硬変などの臓器線維症の病態はコラーゲンの無秩序な増生と蓄積であり，その治療法の戦略としてコラーゲンの合成と分解の要所が標的とされてきた．コラーゲンの合成抑制では，TGFβ，INFγ，TNFα，HGF等，コラーゲンの転写の促進・抑制にはたらく液性因子のシグナル伝達経路への遮断・介入が，広く取り組まれ，またコラーゲン遺伝子プロモーター領域・転写

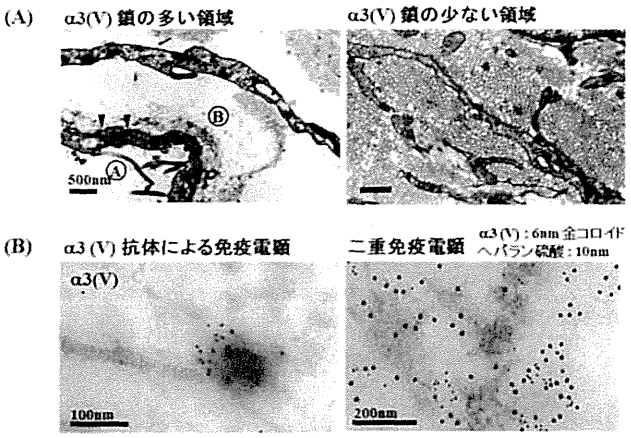

図5　V型コラーゲンα3鎖が線維構築に与える効果

（A）V型コラーゲンα3鎖の多い組織（筋膜直上）と少ない組織（筋より深部）の電子顕微鏡像．α3（V）鎖が多い組織はコラーゲンが細く保たれ，隙間が大きい．最外部の細胞はコラーゲンと接する側Ⓑに基底膜様の構造が形成され（矢頭），反対側Ⓐにはコラーゲンは全く見られず，絨毛状の突起が形成されるなどの形態変化がみられる．Barは500nm．
（B）：左α3（V）特異的抗体による免疫電子顕微鏡解析．α3（V）の局在を示す6nmの金コロイド粒子はコラーゲン線維束の外側にある不定形の付着物質の中にみられる．Barは100nm．右α3（V）抗体（6nm）とヘパラン硫酸糖鎖抗体（10nm）による二重免疫電子顕微鏡解析．両分子は線維束周囲の付着物質に共局在している．Barは200nm．
（住吉秀明，稲垣豊：医学のあゆみ Vol. 244, No 6，医歯薬出版株式会社，2013より出典）

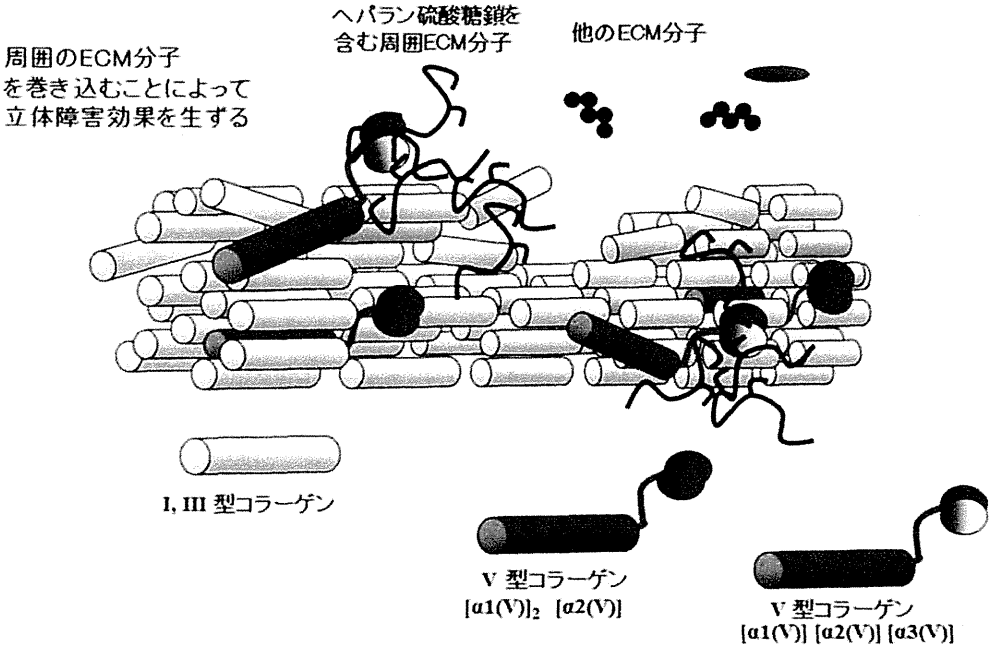

図6 α3（V）を含むV型コラーゲンが線維形成を抑制する仕組み（仮定）
（Lynsenmayer, T. F. et al. J. Cell Biol 1993.（文献2）より改変）

因子群の解析が進められた結果，特異的転写の促進・抑制シグナルに介入し，転写を抑制しうる分子標的薬の開発等の成果に結びついている[8-11]．コラーゲン分解促進においては，線維化した肝臓にコラーゲンを特異的に分解するmatrix metalloproteinases（MMPs）を導入する方法として，骨髄由来細胞を利用する方法が良好な成果を収めている[10,11]．治療への応用の為に，作用機序の異なる方法を組み合わせて用いれば，より効果的であると思われるが，コラーゲンの会合集束過程もまた，有効な線維化抑制ステップになると期待している．コラーゲンは必ずしも結晶が成長するように形成されるわけではなく，生体にはコラーゲンが絶えず生産されているにも関わらず，線維が蓄積させない仕組みがあり，それは自然で理想的な線維化の制御となりうる．その分子的な機序については，まだ手付かずの状態にあるが今回見出されたα3（V）鎖の事例は，その取り掛かりの糸口として期待される．

参 考 文 献

1）van der Rest, M. et al.：Collagen family of proteins. FASEB J., 5：2814-2823, 1991.
2）Lynsenmayer, T. F. et al.：TypeV collagen：molecular structure and fibrillar organization of the chick-α1（V）NH2-terminal domain, a putative regulator of corneal fibrillogenesis. J. Cell Biol., 121：1181-1189, 1993.
3）Wenstrup, J. R. et al.：Type V collagen controls the initiation of collagen fibril assembly. J. Biol. Chem., 279：53331-53337, 2004.
4）Sumiyoshi, H. et al.：Trangsient expression of mouse pro-α3（V）collagen gene（col5a3）in wound healing. Connect. Tissue Res., 53：313-317, 2012.
5）Imamura, Y. et al.：The Pro-α3（V）collagen chain. J. Biol. Chem., 275：8749-8759, 2000.
6）Yamaguchi, K. et al.：Pro-α3（V）collagen chain is expressed in bone and its basic N-terminal peptide adheres to osteosarcoma cells. Matrix Biology, 24：283-294, 2005.
7）Niyibizi, C. et al.：Human placenta Type V collagens. J. Biol. Chem., 259：14170-14174, 1984.
8）Inagaki, Y. et al：Emerging insights into transforming growth factor-β Smad signal in hepatic fibrogenesis. Gut, 56：284-292, 2007
9）Higashi, K. et al.：Interferon-γ interferes with transforming growth factor-β signaling through direct interaction of YB-1 with Smad3. J Biol. Chem., 278：43470-43479 2003.
10）Sakaida, I. et al.：Transplantation of bone marrow cells reduces CCl_4-induced liver fibrosis in mice. Hepatology, 40：1304-1311, 2004.
11）Higashiyama, R. et al.：Bone marrow-derived cells express matrix metalloproteinases and contribute to regression of river fibrosis in mice. Hepatology, 45：213-222, 2007.

European Journal of Immunology

Adipose tissue derived stromal stem cell therapy in murine ConA-derived hepatitis is dependent on myeloid-lineage and CD4$^+$ T-cell suppression

Mami Higashimoto[*1], Yoshio Sakai*[*2,3], Masayuki Takamura[1], Soichiro Usui[1], Alessandro Nasti[1], Keiko Yoshida[1], Akihiro Seki[1], Takuya Komura[1], Masao Honda[3], Takashi Wada[2], Kengo Furuichi[4], Takahiro Ochiya[5] and Shuichi Kaneko[1,3]*

[1] Disease Control and Homeostasis, Kanazawa University, Kanazawa, Japan
[2] Department of Laboratory Medicine, Kanazawa University, Kanazawa, Japan
[3] Department of Gastroenterology, Kanazawa University Hospital, Kanazawa, Japan
[4] Division of Blood Purification, Kanazawa University Hospital, Kanazawa, Japan
[5] Division of Molecular and Cellular Medicine, National Cancer Center Research Institute, Tokyo, Japan

Mesenchymal stromal stem cells (MSCs) are an attractive therapeutic model for regenerative medicine due to their pluripotency. MSCs are used as a treatment for several inflammatory diseases, including hepatitis. However, the detailed immunopathological impact of MSC treatment on liver disease, particularly for adipose tissue derived stromal stem cells (ADSCs), has not been described. Here, we investigated the immunomodulatory effect of ADSCs on hepatitis using an acute ConA C57BL/6 murine hepatitis model. i.v. administration of ADSCs simultaneously or 3 h post injection prevented and treated ConA-induced hepatitis. Immunohistochemical analysis revealed higher numbers of CD11b$^+$, Gr-1$^+$, and F4/80$^+$ cells in the liver of ConA-induced hepatitis mice was ameliorated after the administration of ADSCs. Hepatic expression of genes affected by ADSC administration indicated tissue regeneration-related biological processes, affecting myeloid-lineage immune-mediating Gr-1$^+$ and CD11b$^+$ cells. Pathway analysis of the genes expressed in ADSC-treated hepatic inflammatory cells revealed the possible involvement of T cells and macrophages. TNF-α and IFN-γ expression was downregulated in hepatic CD4$^+$ T cells isolated from hepatitis livers co-cultured with ADSCs. Thus, the immunosuppressive effect of ADSCs in a C57BL/6 murine ConA hepatitis model was dependent primarily on the suppression of myeloid-lineage cells and, in part, of CD4$^+$ T cells.

Keywords: Adipose tissue derived stromal stem cells · Anti-inflammatory effects · CD4$^+$ T cells · ConA hepatitis · Myeloid-lineage cells

Additional supporting information may be found in the online version of this article at the publisher's web-site

Correspondence: Dr. Shuichi Kaneko
e-mail: skaneko@m-kanazwa.jp

*These authors contributed equally to this work.

Introduction

Mesenchymal stromal stem cells (MSCs) are somatic cells that reside in the mesenchymal tissues, such as the BM, umbilical cord, and adipose tissue [1,2]. MSCs are able to differentiate into several types of cells (pluripotent) in the same lineage, such as chondrocytes, osteocytes, adipocytes, and cardiomyocytes, as well as those of different lineages, such as hepatocytes. Because of this differentiation capability, they have been studied as a possible application in regenerative therapy of miscellaneous impaired organs, such as breast reconstruction [3] and repair of ischemic heart tissue [4]. Another intriguing characteristic of MSCs is their immunomodulatory potency [5]. Because most liver diseases, including viral hepatitis [6,7], primary biliary cirrhosis [8], autoimmune hepatitis [9], and steatohepatitis [10], are associated with hepatic inflammatory cells [11], elucidation of the effect of MSCs on hepatic inflammation is important when considering the use of MSCs for treating liver diseases. Although the efficacy of MSC treatment of liver diseases has been reported [12], the detailed immunopathological impact of MSC treatment on liver diseases, particularly for adipose tissue derived stromal stem cells (ADSCs), has not been investigated.

ConA, a plant lectin [13], is frequently used to induce acute hepatitis in rodents [14] to model the pathological features of autoimmune hepatitis. Although this model is mediated mainly by lymphocyte-lineage cells such as T cells and NKT cells, Kupffer cells/macrophages also participate in hepatitis. Therefore, evaluating the therapeutic efficacy of ADSCs in this murine hepatitis model is important. Although the potential efficacy of ADSCs in a BALB/c ConA hepatitis model has been reported [15], the immunopathology has not been investigated.

We confirmed that immediate i.v. administration of ADSCs after ConA injection prevented hepatitis. We also observed that administering ADSCs 3 h after the ConA injection resulted in successful treatment of hepatitis, as the liver was already infiltrated by $CD11b^+$ and $Gr\text{-}1^+$ inflammatory cells. Gene expression analysis of the liver showed that ADSC treatment affected myeloid-lineage cells, providing repair and regenerative effects in ConA-induced hepatitis mice. Moreover, gene expression analysis of hepatic inflammatory cells indicated pathways related to T cells and monocyte-lineage cells. Pathologically important cytokines such as TNF-α and IFN-γ were upregulated in $CD4^+$ T cells isolated from ConA-induced hepatitis mice but were significantly suppressed by co-culture with ADSCs. Thus, the anti-inflammatory effects of ADSCs in the C57BL/6 murine ConA hepatitis model were mediated by the suppression of myeloid-lineage and $CD4^+$ T cells.

Results

Characteristics of the immune response in ConA-induced hepatitis mice

To examine the characteristics of ConA-induced acute hepatitis, we injected 300 μg ConA into C57BL/6 female mice ($n = 4$) and determined serum alanine transferase (ALT) and lactate dehydrogenase (LDH) activities. Serum ALT and LDH activities were elevated through 24 h (Fig. 1A). The macroscopic appearance and histology of the liver obtained 24 h after ConA injection revealed intense necrosis (Fig. 1B). The immunohistochemical analysis showed that the number of $CD4^+$ T cells in the liver peaked at 6 h after the ConA injection, and remained high for 24 h (Fig. 1C and D). The numbers of $CD11b^+$ cells and $Gr\text{-}1^+$ cells accumulated in the liver increased at 3 h and reached a maximum at 12 h after ConA injection (Fig. 1C and D). The numbers of $F4/80^+$ monocyte/macrophage lineage cells increased at 6 h after the ConA injection, but returned to basal levels after 24 h (Fig. 1C and D). We also assessed the frequency of $CD11b^+/Gr\text{-}1^+$ cells, as a phenotype of myeloid-derived suppressor cells (MDSCs), in ConA hepatitis mice at 6 h ($n = 3$). The frequency of $CD11b^+/Gr\text{-}1^+$ cells was higher than that in WT mice (Fig. 1E). Scavenger receptor CD204 expression was higher in $CD11b^+/Gr\text{-}1^+$ cells than $CD11b^+/Gr\text{-}1^-$ cells (Fig. 1F), and the population gated for $CD11b^+$ cells contained granulocytic $Ly\text{-}6C^+/Ly\text{-}6G^+$ cells as well as monocytic $Ly\text{-}6C^+/Ly\text{-}6G^-$ cells (Fig. 1G).

To determine the type of immune-mediating cells involved in ConA-induced acute hepatitis, we depleted mice of various immune cell subpopulations ($n = 4$ per group). Mice that were pretreated with clodronate, a reagent that depletes monocyte-macrophage lineage cells [16], followed by injection of ConA, did not show a significant elevation in serum ALT or LDH activity (Fig. 1H). Mild elevation of serum activity for these enzymes in mice depleted of $CD4^+$ T cells was observed, whereas depletion of $CD8^+$ T cells had no significant effect. These results suggest the importance of monocyte-macrophage myeloid-lineage cells, as well as the contribution of $CD4^+$ T cells, in ConA-induced hepatitis.

ConA-induced acute hepatitis is ameliorated by i.v. administration of ADSCs in vivo

Next, we determined the therapeutic efficacy of ADSCs in the ConA-induced hepatitis model. We obtained and expanded stromal cells from adipose tissue by passaging them eight to ten times (Fig. 2A). Almost all cells expressed the mesenchymal lineage markers, CD29 and CD44 (Fig. 2B). With regard to stem cell markers [17], approximately 40% and 73% of cells expressed CD105 and CD90, respectively (Fig. 2B). Moreover, the cells were pluripotent and were able to differentiate into osteocytes, chondrocytes, and adipocytes (Fig. 2C–F). When 1×10^5 ADSCs were administered via the tail vein immediately after ConA injection in mice ($n = 3$), the elevation of serum ALT and LDH activity was substantially ameliorated, compared with mice without ADSC treatment ($n = 4$) 24 h after injection (Fig. 3A). In terms of therapeutic efficacy, 1×10^5 ADSCs were administered to mice 3 h after ConA injection ($n = 3$), serum ALT and LDH activities were significantly reduced in acute hepatitis mice treated with ADSCs, compared with ConA-induced hepatitis mice without treatment ($n = 4$), 24 h after ConA administration (Fig. 3B). The macroscopic

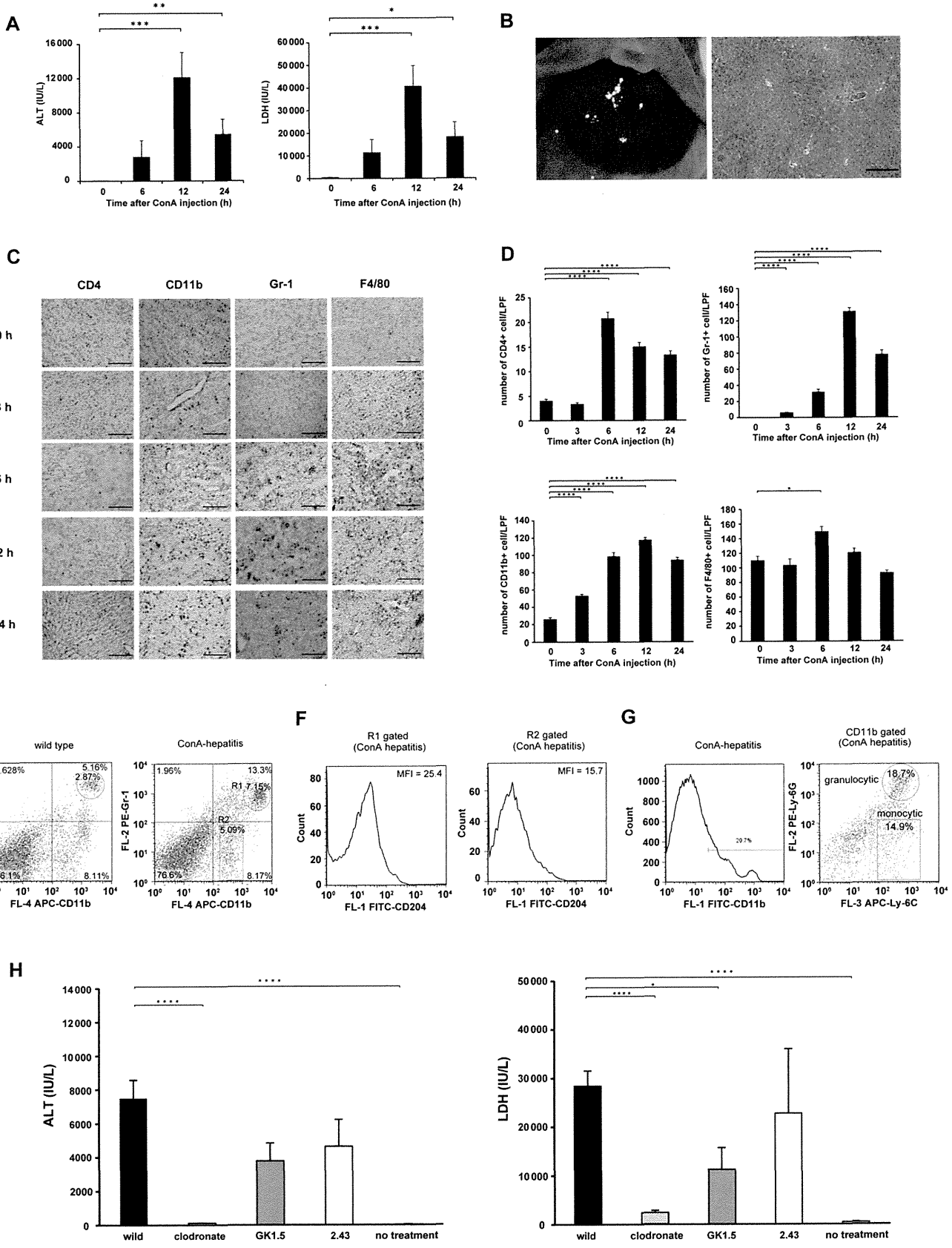

appearance of the liver obtained from mice injected with 300 μg of ConA followed by ADSC administration showed a mild and spotty white area with an almost normal color (Fig. 3C). Liver histology showed an almost normal appearance, with no necrosis (Fig. 3C), indicating that ConA-induced hepatitis was markedly ameliorated by ADSC treatment. No preventive or therapeutic effect on ConA-induced hepatitis resulted from administration of primary cultured murine hepatocytes ($n = 3$); there was no significant reduction in serum ALT or LDH (Fig. 3A and B), macroscopic necrosis appearance, or histological necrosis, compared with ConA-induced hepatitis (Fig. 3C).

ADSC treatment reduces elevated cytokine/chemokine concentrations in ConA-induced hepatitis mice

Marked protective and therapeutic effects of ADSCs on ConA-induced hepatitis were observed. To determine the effect of ADSC treatment on systemic inflammation in ConA-induced hepatitis, we measured serum cytokine and chemokine concentrations in ConA-induced hepatitis mice treated with ADSCs. Mice injected with ConA were immediately treated with ADSCs and serum was collected 6 h after ConA injection ($n = 3$). The elevated serum IFN-γ, IL-2, IL-6, IL-4, IP-10, MIG, KC, and MCP-1 levels in ConA-injected mice ($n = 3$) were significantly reduced by ADSC treatment (Supporting Information Fig. 1A). Injection of mice with ADSCs 3 h after ConA administration ($n = 4$) resulted in significantly reduced serum IFN-γ, IL-2, IL-6, and MIG levels, compared to ConA-injected mice not treated with ADSCs ($n = 6$) (Supporting Information Fig. 1B). Thus, the levels of the array of cytokines and chemokines that are elevated in the sera of ConA-induced hepatitis mice were significantly decreased by ADSC treatment.

Distribution of i.v. administered ADSCs in ConA-induced hepatitis murine models

The distribution of administered ADSCs in ConA-induced hepatitis mice was determined by immunohistochemistry. Administered GFP-expressing ADSCs were observed in the lung, but not the liver, of mice injected with ConA followed by immediate ADSC administration ($n = 6$), through 24 h (Supporting Information Fig. 2A). When administered to mice 3 h after ConA injection ($n = 6$), GFP-expressing ADSCs were observed primarily in the lung, and a few in the liver (Supporting Information Fig. 2B), suggesting that some fraction of ADSCs reached the liver upon occurrence of hepatitis.

Hepatic gene expression changes by ADSCs treatment are associated with Gr-1$^+$ and CD11b$^+$ cells

To investigate the detailed biological features of the liver in ConA-induced hepatitis mice that were treated with ADSCs, we examined the gene expression profiles of liver tissue of ConA-injected mice obtained 2 h after treatment with ADSCs using a DNA microarray. In the liver tissues of mice treated with ADSCs immediately after ConA injection ($n = 3$), 589 gene probes were differentially expressed compared with that in mice with ConA-induced hepatitis that had not been treated with ADSCs ($n = 3$). Expression of the majority of genes was downregulated by ADSCs, as shown by green color ($p < 0.05$; Fig. 4A). Principal component analysis using these genes showed a discernible distribution difference between the ADSC-treated and -untreated groups (Fig. 4B). When mice received ADSC treatment 3 h after ConA injection, hepatic expression of 309 gene probes was altered significantly compared with those in mice with ConA-induced hepatitis that had not been treated with ADSCs ($n = 3$). Expression of the majority of genes was downregulated by ADSCs, as shown by green color ($p < 0.01$; Fig. 4C). Principal component analysis of these genes also showed a discernible distribution difference between the ADSC-treated and untreated groups (Fig. 4D). In the context of biological maps of the genes affected by immediate ADSC treatment, cell differentiation, the inflammatory response, the DNA damage response, and apoptosis predominated (Supporting Information Table 1). In addition to these maps, tissue remodeling and wound repair, mitogenic signaling, and vascular development (angiogenesis) predominated in mice that had received ADSC treatment 3 h after ConA injection (Table 1), indicating that ADSCs provided not only anti-inflammatory effects, but also remodeling effects, in the ConA-damaged liver.

◀ **Figure 1.** Characteristics of ConA-induced hepatitis in C57BL/6 mice. (A–D) C57BL/6 female mice were injected i.v. with 300 μg of ConA. Sera and liver tissues were obtained 3, 6, 12, and 24 h after ConA injection. The data are representative of three individual experiments. (A) ALT and LDH activity in sera. Results are expressed as means ± SE ($n = 4$). $^*p < 0.05$, $^{**}p < 0.01$, $^{***}p < 0.005$ versus 0 h (Student's *t*-test). (B) Representative liver tissues obtained 12 h after ConA injection were assessed macroscopically and microscopically. Magnification: ×100. Bar: 200 μm. (C) Immunohistochemical staining for CD4, CD11b, Gr-1, and F4/80 in the livers of mice for each time point (0, 3, 6, 12, and 24 h; $n = 4$ per time point). Representative images of mice for each time point are shown. Magnification: ×100. Bar: 200 μm. (D) Quantification of the number of CD4$^+$, CD11b$^+$, Gr-1$^+$, and F4/80$^+$ cells in four visual fields per ×100 low-power field in the livers of representative mice in each group. Magnification: ×100. $^*p < 0.05$, $^{****}p < 0.001$ versus untreated mice (Student's *t*-test). (E–G) Hepatic inflammatory cells were isolated from mice 6 h after ConA injection, incubated with fluorescence-conjugated antibodies, and assessed by FACS. Three mice per group per experiment. Experiments were performed twice. (E) Frequency of CD11b$^+$Gr-1$^+$ cells in WT C57BL/6 mice and ConA hepatitis mice. (F) Analysis of CD204 expression in CD11b$^+$Gr-1$^+$ cells (R1-gated region in (E)) and CD11b$^+$Gr-1$^-$ cells (R2-gated region in (E)) among hepatic inflammatory cells from ConA hepatitis mice. MFI: mean fluorescence intensity. (G) CD11b$^+$ cells among hepatic inflammatory cells from ConA hepatitis mouse were gated, and Ly-6C and Ly-6G expression levels in the gated cells were determined. (H) C57BL/6 female mice were injected i.v. with clodronate ($n = 4$), i.p. with anti-CD4 antibody (GK1.5) ($n = 4$), or anti-CD8 antibody (2.43) ($n = 4$) every 24 h for 2 days. The mice were then injected i.v. with 300 μg of ConA. Sera were obtained 24 h after ConA injection, and ALT and LDH activities were then measured. Results are expressed as means +SE ($n = 4$ per group) and are representative of one experiment performed. $^*p < 0.05$, $^{****}p < 0.001$ versus ConA-injected WT mice ($n = 4$) (Student's *t*-test).

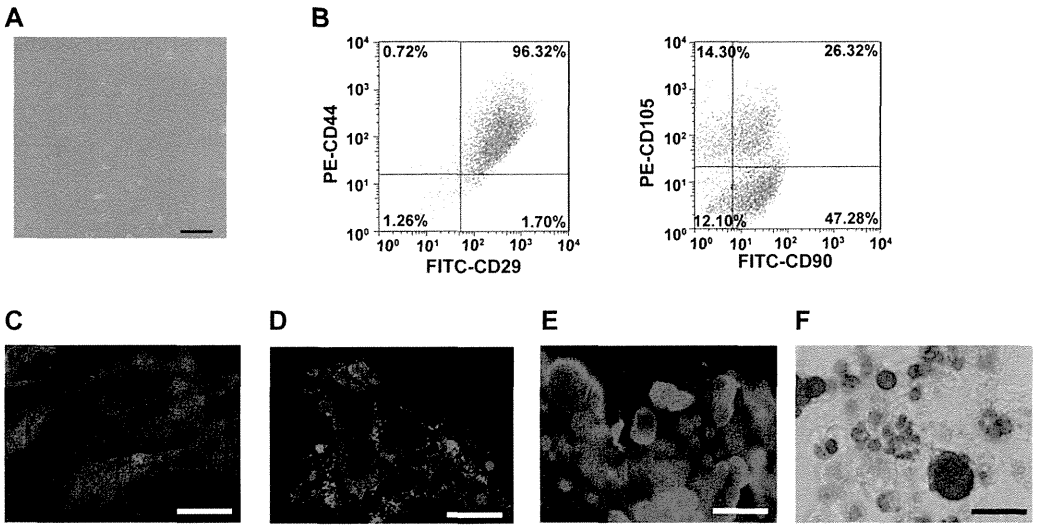

Figure 2. Characteristics and pluripotency of cultured ADSCs. Cells in the stromal fraction of adipose tissues from mice were cultured, maintained, and expanded for eight to ten passages. (A) Spindle shaped cells were observed after eight passages. Magnification: ×100. Bar: 200 μm. (B) Flow cytometric analysis of CD29, CD44, CD90, and CD105 surface marker expression. The data shown are representative of three independent experiments. (C–F) ADSCs were cultured with specific growth factors for induction of osteocytes, chondrocytes, and adipocytes using a mouse mesenchymal stem cell functional kit. Immunohistochemical staining was performed with (C) anti-osteopontin antibody for osteocytes, (D) anti-collagen II antibody for chondrocytes, and (E) anti-FABP antibody as well as (F) Oil-Red O staining for adipocytes. Magnification: x200. Bars: 50 μm. All data shown are from one experiment representative of two independent experiments performed.

Next, we investigated the relevance of these altered genes in the context of inflammatory cells using the public gene expression database of hematopoietic cells and stem cells (GSE27787). The annotated genes among the 589 gene probes detected by microarray analysis probes in the livers of mice that received ADSC treatment immediately after ConA injection were not relevant to any hematopoietic cell type (Fig. 4E). By contrast, among the 309 gene probes, the majority of the annotated genes whose hepatic expression in mice that received ADSC treatment 3 h after ConA injection was affected significantly were found to be highly expressed in Gr-1$^+$ cells and Mac1$^+$ (CD11b$^+$) cells — as indicated by the red color (Fig. 4F). Since majority of the 309 gene probes in the liver of ConA hepatitis were downregulated by ADSC treatment, as indicated by green color (Fig. 4C), these results suggested that effects on Gr-1$^+$ and CD11b$^+$ cells were associated with the therapeutic effect of ADSCs 3 h after ConA injection.

ADSC treatment represses inflammatory cell accumulation in ConA-induced hepatitis

To determine the influence of ADSC treatment on the infiltration/accumulation of immune-mediating cells in the liver of ConA-induced hepatitis mice, we assessed by immunohistochemistry the inflammatory cells in the liver tissues of mice injected with ConA followed by ADSC administration at 3 h. Liver tissues obtained at 6, 12, and 24 h (n = 4 each time point) after ConA injection showed reduced accumulation of CD11b$^+$ cells, Gr-1$^+$ cells, and F4/80$^+$ cells after ADSC treatment (Fig. 5). In contrast, the increased number of infiltrated CD4$^+$ T cells in ConA-induced hepatitis mice was not significantly affected by the ADSCs (Fig. 5). Thus, the predominant change in ConA-induced hepatitis mice treated with ADSCs was in the number of myeloid-lineage inflammatory cells, consistent with the hepatic gene expression data.

T-cell involvement in the altered gene expression of hepatic inflammatory cells by ADSCs treatment

To further assess the anti-inflammatory effects of ADSCs in mice with ConA-induced hepatitis, we isolated hepatic inflammatory cells from mice 2 h after ADSC treatment, which was administered 3 h after ConA injection (n = 2) and from mice not treated with ADSCs (n = 2). A total of 939 genes were differentially expressed in hepatic inflammatory cells from ConA-induced hepatitis mice treated with ADSCs. The gene expression profiles associated with ADSC treatment and ConA-induced hepatitis without ADSC treatment were readily distinguishable (Supporting Information Fig. 3A). Pathway map analysis showed that these genes were relevant to biological pathways of oncostatin M signaling via JAK-Stat or MAPK signaling and CCR5 signaling in macrophages and T lymphocytes in the immune response pathway (Supporting Information Table 2). Network analysis of these genes featured a network consisting of AcRIIA, STAT3, Activin A, FTSJD1, and STAT1 at the top (Supporting Information Table 3), which indicated that pathways involving IL-2 and TNF-α, and the STAT1/STAT3 pathway were also involved (Supporting Information Fig. 3B). These results suggest that T cells, as well as antigen presenting/phagocytosis lineages, were the immune-mediating cell populations affected by ADSC treatment.

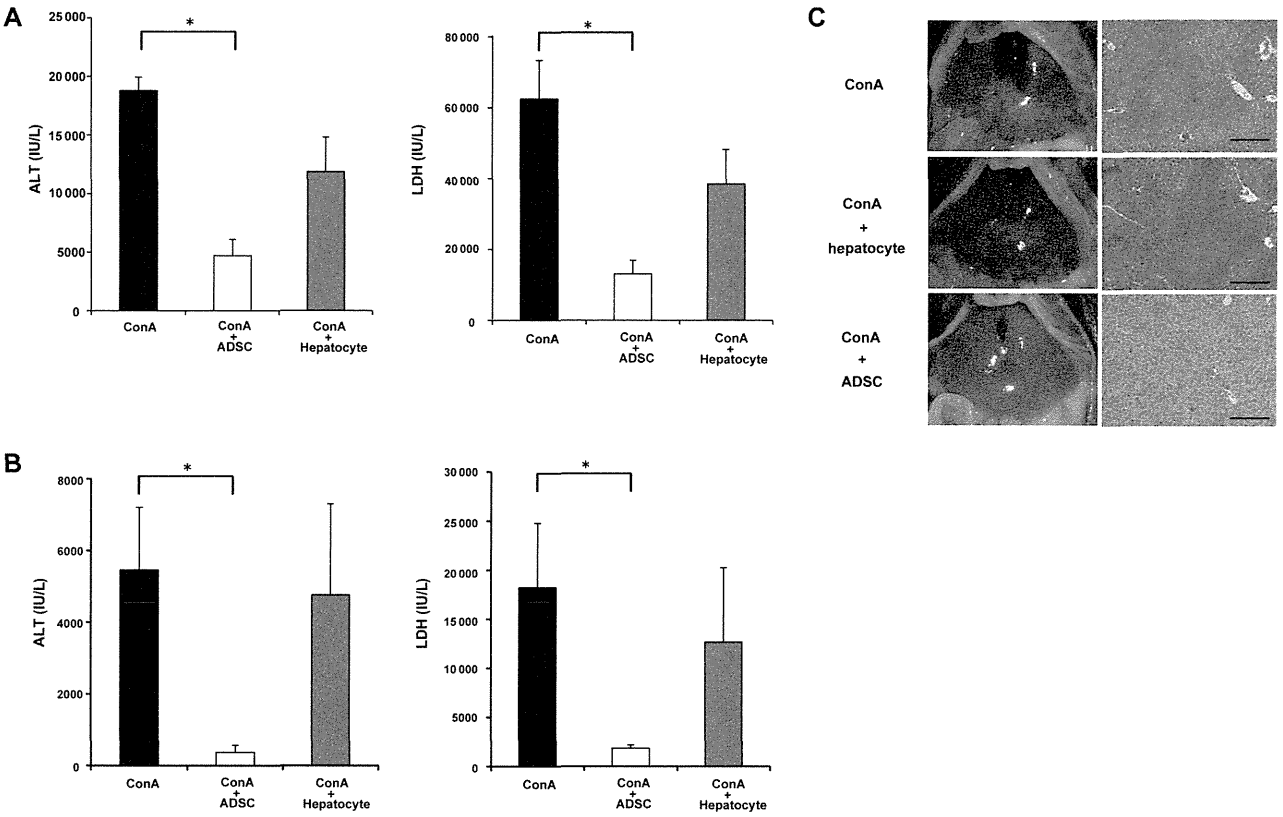

Figure 3. Therapeutic effects of ADSCs in ConA-induced hepatitis. C57BL/6 female mice were injected i.v. with 300 μg of ConA. Immediately or 3 h later, 1×10^5 ADSCs or hepatocytes were injected via the tail vein. Liver tissues and blood samples were obtained 24 h after ConA injection. Liver tissues were examined histologically and serum ALT and LDH activities were measured. (A, B) Serum ALT and LDH activities of mice injected with ConA followed by ADSC injection (A) immediately or (B) 3 h later. ConA: ConA-injected mice without treatment ($n = 4$), ConA + ADSC: ConA-injected mice followed by ADSC treatment ($n = 3$), ConA + hepatocyte: ConA-injected mice followed by primary cultured hepatocyte treatment ($n = 3$). Data are shown as mean ± SE and are from one experiment representative of two independent experiments. $^*p < 0.05$ (Wilcoxon signed-rank test), compared with ConA-injected mice. (C) Macroscopic appearance of the liver (left) and histology of the liver tissues as assessed by H&E staining (right). Magnification of histology: ×100. Bars: 200 μm. Images shown are from one mouse representative of three to four mice from each group studied.

ConA-activated CD4$^+$T cells and CD11b$^+$ cells in the liver are important targets of ADSC treatment

The above data indicated that ADSCs administered in ConA-induced hepatitis had therapeutic immunological effects in terms of repairing the damaged liver and affected CD11b$^+$ and Gr-1$^+$ myeloid-lineage cells and T cells. To further explore how ADSCs affected the subpopulations of inflammatory cells involved in ConA-induced hepatitis, we investigated the expression of cytokine/chemokine-related genes in CD4$^+$ T cells and CD11b$^+$ cells obtained from livers with ConA-induced hepatitis ($n = 4$) that had been treated in vitro with ADSCs ($n = 3$). Expression of TNF-α, IL-10, and CXCL10 was significantly downregulated by ADSC treatment in both CD4$^+$ T cells (Supporting Information Fig. 4A) and CD11b$^+$ cells (Supporting Information Fig. 4B). IFN-γ, IL-4, and CXCL9 expression by CD4$^+$ T cells were significantly affected by ADSCs. Although CCL3, which was upregulated by ConA injection, was not significantly affected by ADSCs, the expression of its cognate receptor, CCR5, was decreased in CD4$^+$ T cells (Supporting Information Fig. 4A), suggesting an effect on the CCL3-CCR5 axis. These results suggest that CD4$^+$ T cells and myeloid-lineage CD11b$^+$ cells were the susceptible hepatic inflammatory subpopulations of cells in the ConA-induced hepatitis liver.

Anti-inflammatory effect of ADSCs on ConA hepatitis do not rely on MDSCs

We further assessed whether the anti-inflammatory effect of ADSCs in ConA hepatitis relied on MDSCs. Neither the frequency of nor the NO production by CD11b$^+$Gr-1$^+$ cells were increased by ADSC treatment (Supporting Information Fig. 5A). CD11b$^+$Gr-1$^+$ cells from ConA-injected mice treated with ADSCs showed arginase activity similar to that in CD11b$^+$Gr-1$^+$ cells from ConA-injected mice (Supporting Information Fig. 5B). CD11b$^+$Gr-1$^+$ cells from ConA-injected mice treated with ADSCs suppressed the ConA-stimulated proliferation of T cells in vitro, although the effect was slightly attenuated compared to that of cells from mice with ConA-induced hepatitis (Supporting Information Fig. 5C). Thus, ADSC treatment was not dependent on MDSCs induced by ConA hepatitis.

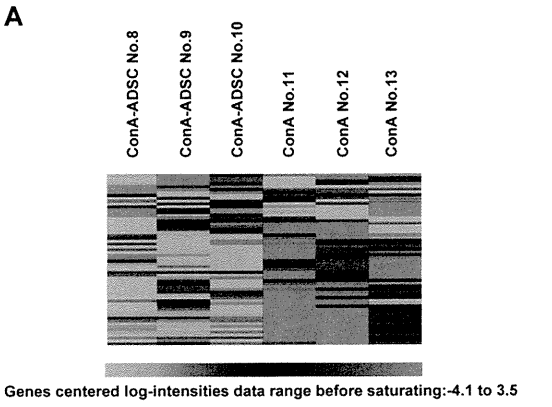

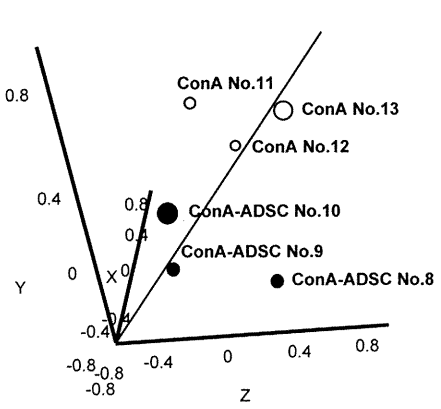

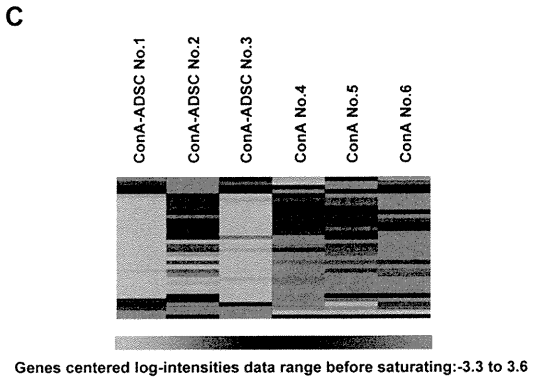

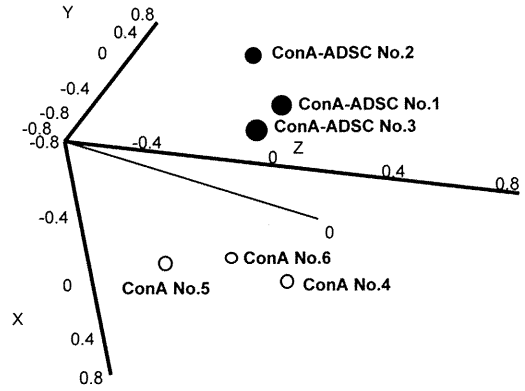

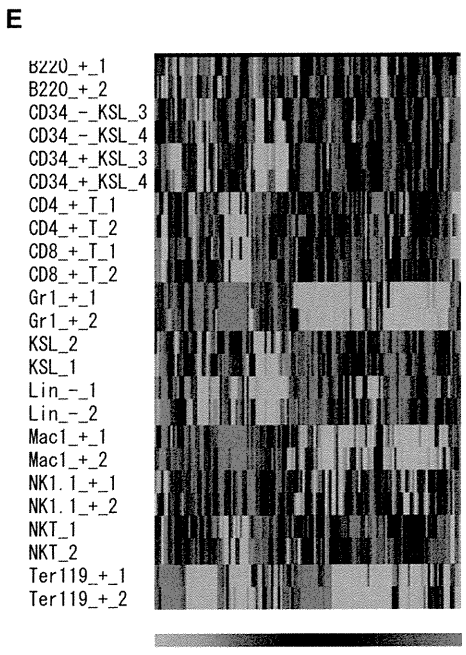

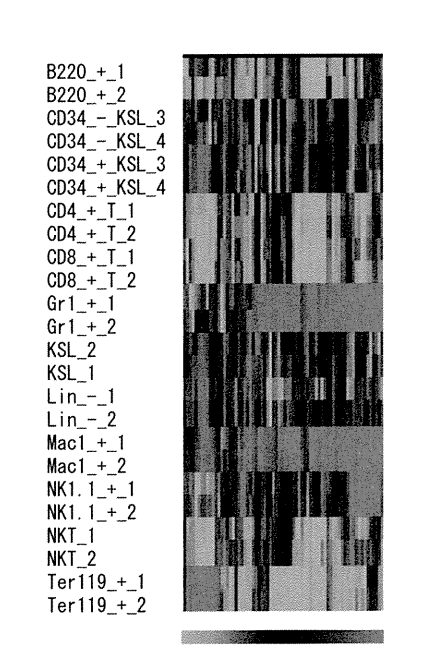

Discussion

MSCs are effective for immune-mediated disease treatment including the ConA-induced BALB/c murine hepatitis model [15], but the detailed mechanisms have not been fully elucidated. Here, we confirmed that ADSCs have preventive and therapeutic effects in a ConA-induced C57BL/6 hepatitis murine model and assessed the immunopathological mechanisms by determining the participating hepatic immunomodulatory cells. ADSCs injected via the tail vein were found in the lung; some were observed in the liver but only when ADSCs were administered 3 h after ConA injection, a time at which infiltration of $CD11b^+$ and $Gr\text{-}1^+$ inflammatory cells into the liver had already begun. Gene expression analysis of liver tissue from ConA-induced hepatitis mice showed that the ADSC treatment induced biological pathways indicative of liver repair and regeneration. Myeloid-lineage cells were the predominant population in terms of affected genes, consistent with immunohistochemical staining of the liver for immune-mediating cells. Furthermore, the gene expression profiles of hepatic inflammatory cells from ConA-induced hepatitis mice treated with ADSCs suggested T-cell and macrophage involvement. Moreover, the expression patterns of cytokine/chemokine-related genes in hepatic inflammatory cells co-cultured with ADSCs suggested that $CD4^+$ T cells were important in ConA-induced hepatitis and were affected by ADSC treatment.

The immunopathological features of ConA-induced hepatitis have been characterized as being primarily lymphocyte-lineage cell-mediated hepatitis [18–20], leading to massive hepatocellular degeneration, necrosis, and apoptosis [21]; thus, this model is relevant to clinical autoimmune hepatitis. Additionally, Kupffer cells play an important role in induction of hepatitis [22]. Unexpectedly, we observed prominent increases in $CD11b^+$, $Gr\text{-}1^+$, and $F4/80^+$ cells in liver tissues of the ConA-induced hepatitis mice. Additionally, we found that the monocyte-macrophage lineage cells contributed most significantly to hepatitis, as confirmed by depletion treatment, such that hepatitis was almost completely abolished when those cell types were abrogated by clodronate. This is further evidenced by the fact that ADSC treatment reduced the number of $CD11b^+$, $Gr\text{-}1^+$, and $F4/80^+$ cells in the liver of ConA-induced hepatitis mice (Fig. 5). The importance of $Gr\text{-}1^+$ and $CD11b^+$ cells was also suggested by changes in the gene expression profile of the liver of ConA-induced hepatitis treated with ADSCs (Fig. 4C and F). Thus, monocyte-macrophage lineage cells are important in the pathogenesis of ConA-induced hepatitis in mice and are important targets of ADSCs. $CD4^+$ T cells were also involved since their depletion partially ameliorated ConA-induced hepatitis. The number of infiltrating $CD4^+$ T cells in the liver of ConA-induced hepatitis mice was not markedly reduced by ADSC treatment. However, gene expression analysis of hepatic inflammatory cells in ConA-induced hepatitis mice treated with ADSCs showed that signaling of oncostatin M, a type I cytokine associated with developing T cells [23], and CCR5 signaling in macrophages and T lymphocytes were affected. Therefore, $CD4^+$ T cells participate as an immune mediator and therapeutic target of ADSCs in the pathology of ConA-induced hepatitis mice.

With regard to cytokine/chemokine-related gene expression in hepatic inflammatory cells of ConA-induced hepatitis mice, expression of TNF-α, IL-10, and CXCL10 in $CD4^+$ T cells and $CD11b^+$ cells was downregulated by ADSC treatment (Supporting Information Fig. 4). Additionally, IFN-γ, IL-4, and CXCL9 were also significantly downregulated in $CD4^+$ T cells, but not in $CD11b^+$ cells (Supporting Information Fig. 4). Changes in the expression of the Th2 cytokines, IL-10 and IL-4, were considered to be the secondary consequence of ConA-induced hepatitis, mediated by TNF-α and/or IFN-γ, which are characterized as Th1-associated cytokines [24]. CCR5 expression by $CD4^+$ T cells was downregulated by ADSCs, which may be relevant to the biological processes indicated by the downregulated genes in hepatic inflammatory cells. Because CCR5 is a $CD4^+$ T-cell receptor that interacts with APCs, such as macrophages [25], suppression of CCR5 expression on $CD4^+$ T cells by ADSC might explain the amelioration of ConA-mediated hepatitis. Overall, the therapeutic efficacy of ADSCs impacted both $CD4^+$ and $CD11b^+$ cells in terms of alteration of levels of inflammatory humoral mediators and cytokine/chemokine profiles, thus contributing to amelioration of ConA-induced hepatitis.

A proportion of i.v. administered ADSCs were present in the livers of ConA mice injected with ADSCs at a time point at which the liver had already been infiltrated with $Gr\text{-}1^+$ and $CD11b^+$ cells, whereas no ADSCs were present in the livers of mice injected with ConA following immediate treatment with ADSCs. This indicates that a liver undergoing inflammation attracts administered ADSCs. The extent of inflammation required to recruit ADSCs should be clarified, as it has previously been reported that hepatitis occurring just 30 min after ConA injection results in recruitment of a substantial number of stem cells to the liver in the BALB/c ConA hepatitis model [15]. Given that the migratory capabilities of MSCs are well known although not yet fully investigated [26], how ADSCs are recruited to an already inflamed liver as a result of ConA administration should be examined. In addition, the ADSCs administered to C57BL/6 mice immediately after ConA injection resided in the lung. In spite of the fact that they were not detected in the liver, these ADSCs prevented ConA hepatitis, indicating the remote effect of ADSCs. Thus, indirect mediators produced by ADSCs associated with their anti-inflammatory effects should be investigated intensively.

◀ **Figure 4.** Gene expression analysis in the liver of ConA-induced hepatitis mice treated with ADSCs. C57BL/6 female mice were injected i.v. with 300 μg of ConA. (A, B, and E) Immediately or (C, D, and F) 3 h after ConA injection, mice were treated with 1×10^5 ADSCs via the tail vein ($n = 3$ each). Liver tissues were analyzed 2 h after ADSC administration and RNA was isolated for gene expression analysis using a DNA microarray. Data shown are from one experiment performed. (A, B) One-way clustering analysis (A) and principal component analysis (B) of the 589 differentially expressed genes in treated and untreated ConA-injected mice. (C, D) One-way clustering analysis (C) and principal component analysis (D) of the 309 differentially expressed genes in treated (after 3 h) and untreated ConA-injected mice followed. Colors indicate the intensity of gene upregulation (red), downregulation (green), and no change (black). (E, F) One-way clustering analysis of gene expression in hematopoietic and stem cells (GSE27787) for annotated genes among the 589 (E) and 309 (F) genes.